EFFECT OF BINDER AMOUNT AND CALCINATION TEMPERATURE ON THE PHYSICAL AND MECHANICAL PROPERTIES OF PRESSED METAL ORGANIC FRAMEWORK UIO-66

A Thesis
Presented to
The Academic Faculty

by

Kenechukwu A. Onubogu

In Partial Fulfillment
of the Requirements for the Degree
Master of Science in the
School of Chemical and Biomolecular Engineering

Georgia Institute of Technology
May 2014

EFFECT OF BINDER AMOUNT AND CALCINATION TEMPERATURE ON THE PHYSICAL AND MECHANICAL PROPERTIES OF PRESSED METAL ORGANIC FRAMEWORK UIO-66

Approved by:

Dr. Krista S. Walton, Advisor
School of Chemical and Biomolecular Engineering
Georgia Institute of Technology

Dr. David S. Sholl, Advisor
School of Chemical and Biomolecular Engineering
Georgia Institute of Technology

Dr. Ryan P. Lively
School of Chemical and Biomolecular Engineering
Georgia Institute of Technology

Date Approved: December 3, 2013

To my family and loved ones

ACKNOWLEDGEMENTS

First and most importantly, I give special thanks to God for His grace and blessings throughout my life. The Lord has been so good to me in many ways especially during my studies and without Him I would not have accomplished anything.

I would like to express my sincerest gratitude to my research advisors, Dr. Krista S. Walton and Dr. David S. Sholl, for their guidance, instructions and encouragement throughout the duration of this work. Their dynamism, vision and priceless advice during the duration of my research greatly enhanced my thought process as a researcher and analysis of technical problems. It was a great honor working with them and I will forever be grateful for such opportunity. I would also like to thank Dr. Ryan Lively for accepting to be a member of my thesis committee and providing insight into my work.

I am grateful to every member of the Walton and Sholl groups for their generous contributions and critiques to my work. Nick Burtch, Mike Mangarella and Greg Cmarik provided the trainings needed for the operations of the various equipment used in this work. Will Mounfield assisted in designing the sample holder needed for measuring crush strength of pellets and Dr. Bogna Grabicka did an excellent job in making me feel at home and ensuring safety and organization in all laboratories. I also acknowledge Dr. Richard Neu and James Huggins from the George W. Woodruff School of Mechanical Engineering, Georgia Tech, for allowing me use their laboratory and equipment for taking crush strength measurements.

Finally, I am extremely gratefully to my entire family for their endless love, care and sacrifice especially to my parents who always supported me in every way possible in

ensuring that my dreams became a reality. To all my friends and well-wishers who never stopped encouraging and believing in me even during my various trying moments, I say thank you.

TABLE OF CONTENTS

LIST OF TABLES

LIST OF FIGURES

LIST OF SYMBOLS AND ABBREVIATIONS

~	Approximately
Kα	K-alpha
λ	Wavelength
θ	Angle of Incidence
%	Percentage
cc	Cubic Centimeters
cu	Copper
g	Gram
GO	Graphite Oxide
in	Inch(es)
K	Kelvin
kV	Kilovolt
mA	Milliampere
min	Minute(s)
mg	Milligram
mm	Millimeters
mmol	Millimole
PVA	Polyvinyl Alcohol
pXRD	Powder X-Ray Diffraction
rpm	Revolutions per Minute
TA	Tartaric Acid
UiO	University of Oslo
wt%	Weight Percent

SUMMARY

Metal-organic framework (MOF) materials are a novel set of porous crystalline materials that have generated great scientific interest within the past two decades due to their attractive properties such as high porosity, surface areas and tunable pore structure. These properties have made them emerge as potential candidates suitable for a broad range of applications such as gas separations and storage, catalysis and drug delivery. Despite their fascinating properties, MOFs are often unsuitable for most industrial applications due to their instability when exposed to mechanical stress. The challenge therefore is to convert the MOFs to high strength materials capable of withstanding such stress while still maintaining their exciting properties.

This thesis thus focuses on investigating the effects of different binders on a zirconium based metal-organic-framework, UiO-66, in an attempt to enhance the mechanical strength of the adsorbent samples. Three different binders, kaolinite, polyvinyl alcohol and tartaric acid, are mixed with the parent MOF material in different weight percents, pressed into solid disc pellets at different pressures and calcined at different temperatures. Properties such as changes in structure, density, porosity, surface area, radial crush strength, and the adsorption capacity with CO_2 are measured and evaluated.

Results gathered from this work reveal that polyvinyl alcohol is the most promising of the three binders due to the increase in the strength of pellets and the slight decrease in CO_2 adsorption it offers. Recommendations for future research work aimed at

driving these materials towards reaching their maximum application potentials are proposed.

CHAPTER 1

INTRODUCTION

Metal organic frameworks (MOFs) are a relatively novel microporous crystalline class of materials capable of forming one, two, or three dimensional networked structures composed of metal ions as center and organic ligands as linkers. In addition to being very porous, they also possess other attractive properties Their porosity is beneficial for the filtration and separation of gases , which is a common and important industrial process. Their high surface areas [1] makes them suitable for gas storage applications and their tunable pore structures and chemical functionality make them very useful from a synthesis point of view. They thus possess potential industrial applications in gas adsorptions[2, 3], separations[4], storage[5, 6], catalysis[7] and drug delivery[8]. As such, they have attracted huge research interest over the past two decades due to their emergence as materials that can potentially replace traditional inorganic porous adsorbents such as zeolites and activated carbons

A common issue with synthesized MOFs is that they are usually generated as small crystals or powders, which cannot be used for most industrial applications due to their low packing density. Most industrial applications usually involve loading and pneumatic transport whereby materials are exposed to high mechanical stress. Particles are often exposed to diverse mechanical strains during transportation, charging to reactors and operations. In a fixed bed reactor, particles must withstand pressure caused by erosion by high velocity gas streams[9]. Packed bed reactors are usually filled with pellets of higher packing densities in order to avoid large pressure drops during gas phase separations [10]. In moving bed reactors, particles must resist attrition from rubbing against each other and from colliding with walls of reactor[9]. Performance of these particles under these stringent conditions depends heavily on their mechanical strength

and their ability to maintain their porosity. As such, the powders must be transformed into forms that are strong enough to withstand the forces acting on them. Such strength must be high enough to not only ensure structural stability of the material but to also prevent dusting that arises from forces simulated on the material during handling and transportation. There is thus a need for MOFs to be extruded or pressed into forms suitable for various applications.

Although extruding is less expensive than pelletizing[9], pelletizing is the more commonly used method for forming these shaped bodies for two main reasons. First, extrudates have less resistance to abrasion than pellets[9]. Secondly, the use of screw extrusion does not allow for the generation of high pressures, which is not suitable for masses that require high extrusion force. Even after being formed into pellets, MOFs may not exhibit sufficient strength, as they are still very well less mechanically stable than their inorganic counterparts, zeolites[11]. Binders can therefore be added to increase the strength of MOF pellets. Binders also reduce the adversity of conditions that would otherwise be required by reducing the pressure and temperature needed to form high quality pellets[12]. The general process involved in forming pellets with binders is as follows:

a. Mixing: Here adsorbent samples and binders are mixed in proportions that will give desired properties.
b. Pasting: This involves the use of viscosity enhancing substances as binder plasticizers to ensure proper agglomeration for mechanical stability. Agglomeration simply involves forming bigger particles from smaller ones. Usually particles are held together as agglomerates by binding forces when particles in moist state are brought in contact with each other during agitation. Capillary forces brought by wetting with aqueous solution is the most common

mechanism[13]. An appropriate amount of plasticizer must be used to ensure proper agglomeration.

c. Pressing: Samples are pressed into pellets at different forces to form high strength compacts.
d. Drying: Pellets are dried in an oven in a controlled manner. This is important especially for samples with clay binders where exposure to high temperatures for longer periods of time could lead to clay shrinkage and cause fissures on the pellets during the calcination step[14].
e. Calcination: This is the last stage of the process where pellets are heated at much elevated temperatures under the presence of air. Calcination helps eliminate extraneous materials like volatile and unstable ions that may have been introduced but are not desired in the final material[15]. In addition, it improves the strength of the final pellet by causing incipient sintering. Excessive sintering causes reduced activity and diffusional limitations caused by a reduction in surface area and pore size[15].

Some research has been done previously on pelletizing a number of MOFs with and without binders [6, 10, 16-19] and examining the changes in crystal structure of MOFs after the application of pressure.[20, 21]. However, most MOFs have been shown to experience significant structural degradation under compression at high pressures.[16, 19] A zirconium based metal-organic framework, UiO-66, was recently shown to withstand this effect at higher pressures[19]. UiO-66 also recently attracted attention due to its stability in air and most chemical solvents [2] UiO-66 is therefore a suitable MOF for this study. Compared to other MOFs, UiO-66 possesses excellent mechanical stability and resistance to shear stress [11]. Not much work has been done on investigating ways

to improve the mechanical strength of UiO-66 up to a level comparable to that of zeolites while still retaining some its attractive properties

The increase in the concentration of greenhouse gases such as carbon dioxide (CO_2) in the atmosphere over the past few decades caused by the rapid increase in energy consumption is an alarming concern due to its adverse effect on our climate and environment. The mitigation of CO_2 emission by carbon capture technology has thus become an area of intense research over the past few years [22-25]. MOFs have been considered for this application due to their high selectivity over other gases and their high storage[22]. For MOF composites made with binders to be readily applicable for this application, investigations would need to be carried out to observe the extent by which CO_2 adsorption is affected with these composites.

The objectives of this study were to:

1. Study the effect of different binder types, binder compositions, calcination temperatures and pelletization pressure on the textural and mechanical properties of the parent adsorbent sample. Properties such as changes in structure, bulk density, radial crush strength, surface area and porosity were measured and evaluated.
2. Study the adsorption performance of CO_2 with respect to the conditions aforementioned and decide on how a balance could be made between the mechanical strength and adsorptive properties of UiO-66.

A tradeoff is usually associated with improving the strength of UiO-66 pellets. The use of binders typically affects the textural properties of MOFs and results in loss of

adsorption capacity due to the partial pore blocking and reduction in accessible pore volume. This could even be made worse depending on the extent of application of some of the conditions stated in the first objective above. The second aim given above seeks to obtain suitable conditions by which this unfavorable situation is minimized by maintaining a reasonable adsorption power while significantly increasing the mechanical properties of the MOF material.

CHAPTER 2

MATERIALS AND EXPERIMENTAL WORK

2.1 UiO-66 Structural Description

The UiO-66 structure is a zirconium based MOF framework made from centric $Zr_6O_4(OH)_4$ octahedra with each zirconium metal center connected to twelve 1,4-benzene-dicarboxylate (BDC) linkers. Each central octahedral cage of diameter 11 Å[26] is linked with eight cornered tetrahedral cages of diameter 8 Å[26] via microporous triangular windows of size range 5 to 7 Å[26] to form a rigid face centered cubic crystal framework (Figure 1) [27].

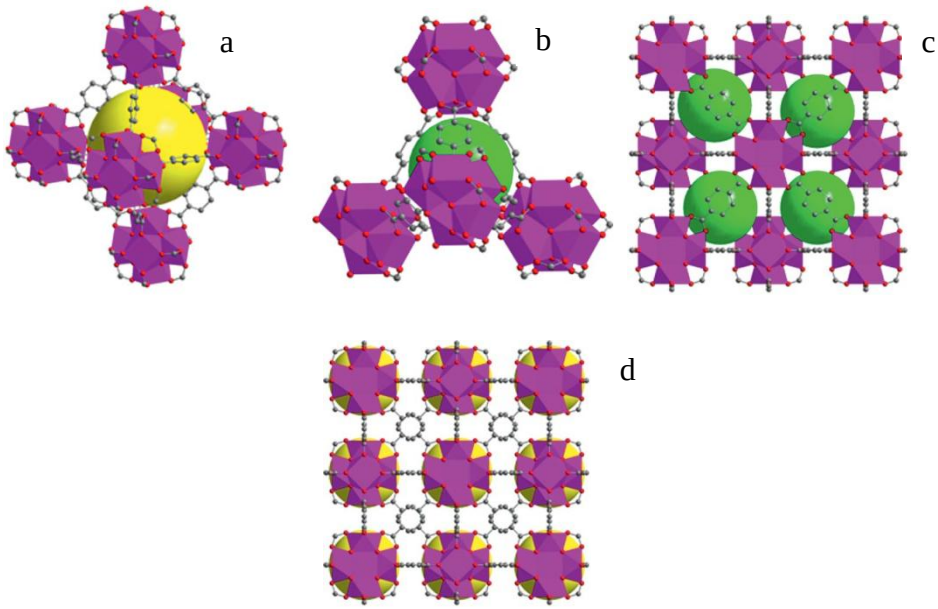

Figure 1: Crystal Structure of UiO-66. (a) Single Octahedral Cage (yellow sphere). (b) Single Tetrahedral Cage (green sphere). (c) Spatial Arrangement of Tetrahedral Cages in Framework. (d) Spatial Arrangement of Octahedral Cages in Framework. Taken with permission from Biswas and Van der Voort [27]

2.2 Materials and Synthesis

The synthesis method used here was the conventional solvothermal synthesis method which involves heating an organic ligand and a metal salt in a solvent at a particular temperature and for a certain period of time. The reported synthesis procedure by Peterson et al.[19] was followed with slight modifications to the amount of starting materials and synthesis time to get a higher yield and better crystals. The as synthesized samples mentioned below are those obtained after synthesis and solvent exchange.

2.2.1 Preparation of UiO-66

The materials used in this study were the as synthesized UiO-66 powdered sample prepared in our laboratory. 61.68 mmoles of zirconium (IV) chloride (ZrCl4) and 61.68 mmoles of terephtalic acid were mixed in 800 ml of dimethyl formamide in a glass beaker. The substrate mixture was then stirred at 300-500 rpm using a stir bar until a homogenous mixture was obtained. The resulting mixture was divided equally into four 400 ml glass jars and placed in an oven at 120 ^{o}C for 48 hrs. At the end of the solvothermal treatment, the solution was cooled to room temperature and the product was washed thrice over a period of three days with DMF and then washed once for one day with methanol to remove any unreacted reactants while collecting the solvent via decantation. The resulting white sample was left to air dry on a filter paper prior to activation under vacuum at 250 ^{o}C.

2.2.2 Sample Preparations With Binders

Three different polymers were used as binders for this study. Kaolinite clay with the chemical formula of $Al_2O_7Si_2.2H_2O$, D-L tartaric acid and polyvinyl alcohol (Mowiol 10-98) were all purchased from Sigma Aldrich.

2.2.2.1 Preparation of UiO-66-Kaolinite sample

Before the kaolinite samples were mixed with the as synthesized UiO-66 sample, thermal gravimetric analysis was carried out on the kaolinite sample to determine the temperature range at which phase change and densification of kaolinite occurs. It is well known that when treated in air at different temperatures, kaolinite undergoes various transitions into forms[28, 29], according to Equations (1), (2) and (3) below, which could further fortify the mechanical strength of adsorbent samples[14].

$$\underset{\text{kaolinite}}{2Al_2\,Si_2O_5(OH)_4} \xrightarrow{500-600^oC} \underset{\text{metakaolinite}}{2Al_2Si_2O_7} + 4H_2O \qquad (1)$$

$$\underset{\text{metakaolinite}}{2Al_2\,Si_2O_7} \xrightarrow{925-950^oC} \underset{\text{spinel}}{Si_3Al_4O_{12}} + SiO_2 \qquad (2)$$

$$\underset{\text{spinel}}{3Si_3Al_4\,O_{12}} \xrightarrow{1050^oC} \underset{\text{mullite}}{2Si_2Al_6O_{13}} + \underset{\text{cristobalite}}{5SiO_2} \qquad (3)$$

Samples of kaolinite were calcined in air at 650 ^oC and 800 ^oC in a Lindberg Blue M furnace from Thermo Scientific. A ramp rate of 10 ^oC/min was used to raise the

temperature from room temperature to the desired temperature after which it was held on at the set temperature for two hours before cooling. For each temperature, 0.039g of the pre-treated kaolinite was added to 0.156 g of UiO-66-S1 such that a 20 weight percent (wt%) portion of the resulting mixture was comprised of the kaolinite binder. The mixtures (UiO-66_K650_20wt% and UiO-66_K800_20wt% respectively) were stirred vigorously until a homogenous mixture was observed (~25 minutes). 0.105 ml of water, corresponding to 35 wt% of total mixture weight was added as plasticizer to assist in mixing and to ensure proper agglomeration of the resulting mixture.

2.2.2.2 Preparation of UiO-66-PVA mixture

PVA is a water soluble synthetic polymer and an excellent adhesive with superior bonding strength and excellent adhesion to both hydrophilic and hydrophobic materials[30]. A fully hydrolyzed PVA grade has 98.5 to 99.2 mole% of its acetate group replaced by alcohol group while a partially hydrolyzed grade has 86 to 89 mole% of its acetate group been replaced by alcohol group[30, 31]. Fully hydrolyzed PVA was used a binder for this study for two main reasons. In partially hydrolyzed PVA, the residual acetate groups reduce crystallinity and results in weaker materials. With fully hydrolyzed PVA, however, the overall high degree of crystallinity is maintained. Also, the extra alcohol groups present in the fully hydrolyzed grade increases the hydroxyl functionality which aids CO_2 adsorption as will be discussed in Chapter 3.

15% PVA/water solution was prepared according to the method described by Finsy et al.[10]. 3.53 g of PVA granules were added to 20 ml deionized water in a round bottom flask fitted with a reflux condenser to prevent loss of water and placed on a

magnetic hot plate stirrer. The solution was heated to 90 ^{o}C to ensure complete dissolution while stirring with a stir bar. Weighed amounts of the PVA/water solution were added to weighed amounts of UiO-66 according to Table 1 below.

Table 1. Composition of Materials Using PVA as a Binder

Designated sample name	**% Weight of UiO-66 in the dried mixture**	**% Weight of PVA in the dried mixture**	**% Weight of water in the original wet mixture**
UiO-66-S1_PVA_7.5wt%	92.5	7.50	42.5
UiO-66-S1_PVA_10wt%	90.0	10.0	36.2
UiO-66-S1_PVA_13wt%	87.0	13.0	29.8

2.2.2.3 Preparation of UiO66-Tartaric Acid Mixture

Weighed amounts of UiO-66 were mixed with weighed amounts of tartaric acid according to Table 2 below. The mixture was stirred vigorously until a homogenous mixture was noticed (~25 minutes). Appropriate amount of water was then added as plasticizer according to Table 2 below and a spatula was used to properly mix the resulting paste mixture.

Table 2. Composition of Materials Using Tartaric Acid as a Binder

Designated sample name	% Weight of UiO-66 in the dried mixture	% Weight of tartaric acid in the dried mixture	% Weight of water in the original wet mixture
UiO-66-S2_TA_7.5wt%	92.5	7.5	48.8
UiO-66-S2_TA_10wt%	90.0	10.0	45.0
UiO-66-S2_TA_13wt%	87.0	13.0	42.5

2.2.3 Pelletization Process

An extrusion press was used as the preferred method for forming shaped bodies. Unlike screw extrusion, the extrusion press allows for the generation of high pressures that are suitable for masses that require high extrusion force. A Carver Manual Pellet Press was used in the preparation of all pellets. 0.3 g of the prepared powdered material was placed in the cylindrical cavity of a 13 mm pellet die and leveled off with a plunger. Forces of 1400 lbs, 2200 lbs and 3600 lbs corresponding to pressures of 6802 psi, 10689 psi and 17491 psi respectively were applied to the cross sectional area (0.2057 in^2) of the

sample for two minutes. The timer was started once the desired force was reached and the clamp pressure was immediately bled out once the two minutes had elapsed. The cylindrical base was removed and replaced with an ejector after which the disc shaped formed sample pellets were pressed out.

2.2.4 Post Pelletization Process

Pellets were dried in a laboratory oven at 393 K for 2.5 hours to remove free water as this helps prevents fissures and cracks during the calcination process. After drying, pellets were placed in the tube furnace and calcined at different temperatures under the flow of air gas and at a ramp rate of 10 ^{o}C/min.

2.3 Characterization

2.3.1 Thermo-gravimetric Analysis and Differential Scanning Calorimetry

Thermal gravimetric analysis (TGA) and differential scanning calorimetry (DSC) were performed on the binders using a Netszch STA 449 F1 Jupiter to examine the thermal degradation of the materials. About 10 mg of sample was loaded onto an alumina crucible and placed on the microbalance and weighed using the internal weight balance. Two mass flow controllers (one protective and one purge mass flow controller), were used to maintain the flow of air at approximately 20 cc/min through the furnace. Samples were heated within the range of 20 to 1100 ^{o}C at a constant ramp rate of 2 K/min in air.

From these, the temperature range at which phase change, decomposition and densification of the binders occurred were gathered from the resulting data.

2.3.2 Powder X-ray Diffraction (PXRD)

Powder X-ray diffraction measurements (PXRD) were performed using an X'Pert Pro PANalytical X-Ray Diffractometer. All samples were scanned at 45 kV and 40 mA, using Cu Kα radiation (λ=1.54 Å) and a step size of 2θ = 0.033 over the 2θ range of 5-50^{o}. PXRD patterns were compared with the published simulated and experimental data of similar materials and patterns were processed using PANalytical X'pert HighScore.

2.3.3 Adsorption Tests

2.3.3.1 Nitrogen Adsorption Measurements

The specific surface area and the micropore volume of adsorbents are two important properties because materials with a larger amount of these properties are often preferred in separation and purification processes. Attention was focused on these properties when taking nitrogen adsorption measurements The surface area is strongly correlated with the amount of adsorbate to be adsorbed at the adsorption sites[32]. The micropore volume determines the adsorptive capacity and frequency of regeneration of adsorbent required during adsorption – desorption cycles[32]. The Dubinin-Radushkevich (D-R) method, which is based on Polanyi and Goldmann's potential theory and valid for purely microporous solids[32], was used in the determination of the micropore volume while the Brunauer Emmett Teller (BET) method was used to determine the specific surface areas of the test materials.

2.3.3.1.1 Preparation of Samples (Outgassing)

During sample synthesis, some gases become physically adsorbed to the surface of the material. This reduces the amount of nitrogen gas to be adsorbed, hence reducing the specific surface area of the sample. It is therefore essential to remove these gases prior to any adsorption measurement. Outgassing was performed on 20-30 mg samples at 250 ^{o}C for 12 hours using a Quantachrome Flovac Degasser under dynamic vacuum by Quantachrome Instruments.

2.3.3.1.2 Isotherm Analysis

After samples were activated, they were reweighed and the masses were recorded for adsorption analysis. Nitrogen adsorption isotherms were measured at 77 K over a range of relative pressures from 10^{-6} to 0.997 using a Quantachrome SI Surface Area and Pore Size Analyzer. The BET analysis which was derived for multilayer gas adsorption at temperatures close to their condensation points was the method used to determine the surface areas of these porous materials from the nitrogen adsorption isotherms

2.3.3.1.3 BET Theory and Specific Surface Area Determination

Physisorption arises from the Van der Waals forces between the gas molecules and the adsorbent's surface. The BET model which accounts for multilayer adsorption was used to estimate the surface area and has the resulting BET equation (Equation4).

$$\frac{p}{v(p_o - p)} = \frac{c-1}{v_m c}\frac{p}{p_o} + \frac{1}{v_m c} \qquad (4)$$

where,

p = partial vapor pressure of adsorbate gas in equilibrium with the surface at 77 K

p_o = saturation pressure of adsorbate gas at 77 K

v = volume of gas adsorbed at standard temperature and pressure

v_m = volume of gas adsorbed to produce a monolayer on the surface of the solid sample

c = BET constant, related to the heat of adsorption of the adsorbate gas on the sample

From equation (4), $p/(v(p_o - p)$ is plotted against p/p_o to yield a linear region over the range $0.05 < p/p_o < 0.3$. For the data to be considered acceptable, the linear region should have a positive y-intercept equal to $1/v_m c$ with a the value of c being greater than zero and the selected pressure range should have values for $v/(p_o - p)$ increasing with p/p_o[33].

v_m is calculated as $1/(slope + intercept)$, the slope being equal to $(c - 1)/v_m c$. From these, the surface area S is calculated as:

$$S = \frac{v_m N_A}{v\, m} a \qquad (5)$$

where,

N_A = Avogadro constant (6.022 x 10^{23} molecules/mole)

a = cross-sectional area of an adsorbed nitrogen molecule (16.2 $Å^2$)

m = mass of the adsorbent

2.3.3.2 Single Component Gas Adsorption Measurement

An Intelligent Gravimetric Analyzer (IGA-100 series) from Hiden Isochema Limited was used to measure the adsorption isotherms for carbon dioxide at 293 K for

pressures up to 15 bar. Prior to adsorption measurements, activation was carried out in situ under vacuum at 493 K until there was no sample weight losses observed. 35 to 50 mg of samples were used for all measurements and an equilibration time of 30 min was used for each point in the isotherm.

2.3.4 Mechanical Tests

2.3.4.1 Bulk Crush Strength

Tests for bulk crush strength were carried out using a DDL 650M test equipment from DDL Inc., which has a compressive force limit of 1000lbs The side (radial) crush strength of the pellets was measured according to the ASTM standard test method for radial crush strength measurements[34]. Pellets were placed between two steel anvils with very flat and smooth surfaces. Due to difficulty in keeping these pellets (1.2 to 2.6mm thick) vertically upright, a specially made sample holder was used to hold these pellets in place and maintain a constant contact area. The anvils were lowered just until minimum contact was made with the pellets to keep it in place, at which point the sample holder was removed. Increasing force at a uniform ramp rate of 0.05 in/min was applied until the first complete disintegration of the pellet was observed (Figure 2). Each test was done for 2-3 identical pellets and the average forces were read and recorded to the nearest one hundredth of a pound. The anvils were separated and properly cleaned with a soft clean cloth to get it ready for the next test.

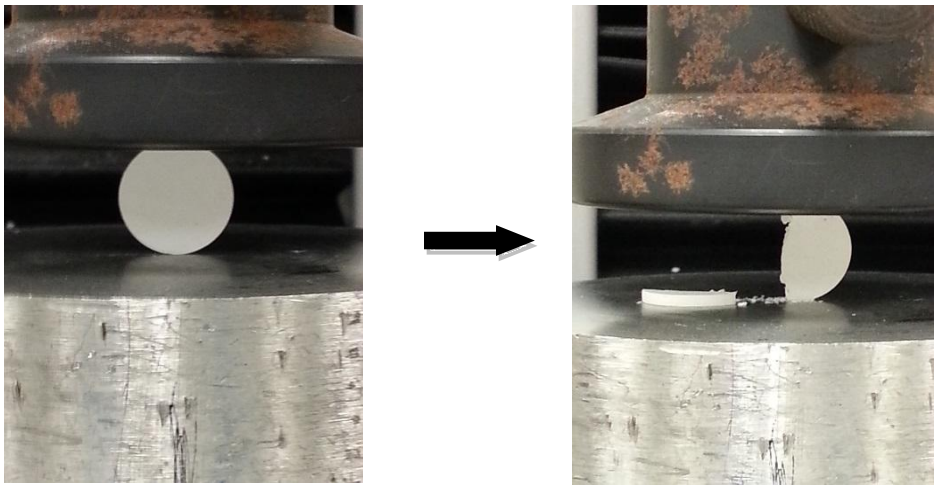

Figure 2: Disintegration of a Pellet.

2.3.4.2 Bulk Density Measurements

The bulk density of the powders was measured by placing a weighed amount of powder in a graduated cylinder and pressing it down to level it off. The volume of the sample was read from the graduated cylinder and the bulk density was simply calculated as:

$$Density = \frac{mass}{volume} \qquad (6)$$

The bulk density of the pellets was measured by measuring the weight of the pellets at their final states and recording their thickness using a digital vernier caliper. The density was then calculated using the Equation 6 above.

CHAPTER 3

RESULTS AND DISCUSSION

3.1 UiO-66 Studies

3.1.1 Synthesis and Pelletization of UiO-66

Two different batches of UiO-66 were synthesized for this work (UiO-66-S1 and UiO-66-S2). The textural properties of both samples are summarized in Table 3. The surface area of UiO-66-S1 is similar to the previously reported experimental values in literature [19, 35] and is slightly less than the reported theoretical surface area (1186 m^2/g)[36]. The batches were prepared four weeks apart with different $ZrCl_4$ samples. This could be a reason why such a difference in surface areas was observed between both batches. Samples of UiO-66-S1 were pelletized (without binder) at 6802 psi, 10689 psi and 17491 psi (UiO-66-S1_6802 psi, UiO-66-S1_10689 psi and UiO-66-S1_17491 psi) to investigate the effect of pelletization pressure on the textural properties of UiO-66. A slight decrease is noticed in the surface areas and micropore volume of the pressed samples compared to the parent powdered MOF sample. During the pelletization process at the initial pressure of 6802 psi, there was a notable drop in micropore volume. As pressure increases, the crystallites get much closer to each other and some of the mesopores initially formed are converted to additional micropores, resulting in the observed increase in microporosity at the higher pelletization pressure.

Table 3. Textural Properties of the As-Synthesized UiO-66 Batches

Sample	BET Surface Area (m^2/g)	Pore Volume (cc/g)	Micropore Volume	% Micropore Volume
UiO-66-S1	1033	0.79	0.54	70.4
UiO-66-S1_6802psi	904	0.71	0.45	63.7
UiO-66-S1_10689psi	910	0.65	0.440	67.4
UiO-66-S1_17491psi	963	0.60	0.44	73.0
UiO-66-S2	1254	0.63	0.54	86.0

3.1.2 Thermolysis of UiO-66

TGA was performed to determine the temperature stability of UiO-66. This was important for determining an appropriate calcination temperature limit for all binder treated MOF samples. Figure 3 shows that the as-synthesized UiO-66 is thermally stable up to 430 ^{o}C. This was the same temperature recorded by Biswas et al.[37].

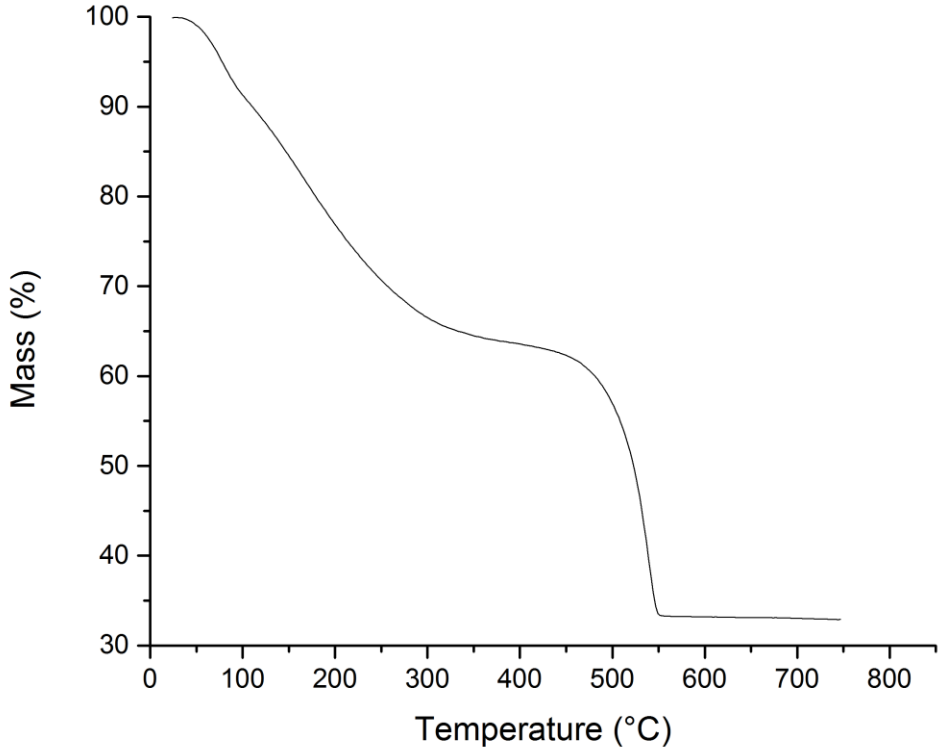

Figure 3. TG Curve for Activated UiO-66

3.2 UiO-66-Kaolinite Studies

3.2.1 Thermolysis of Kaolinite Sample

TGA was performed on kaolinite to examine the thermal degradation of the sample as shown in Figure 4. Within the temperature range 440-600 ^{o}C, dehydroxylation of kaolinite and formation of metakaolinite takes place, while at about 1000 ^{o}C, densification occurs and mullite is formed as shown by the exothermic peak. At 524 ^{o}C, there is an endothermic peak which may be attributed to the dehydroxylation of kaolinite and formation of metakaolinite[28]. Due to the formation of metakaolinite above 600 ^{o}C,

kaolinite samples were pre-treated thermally at 650 and 800 ^{o}C before being added as a binder to UiO-66.

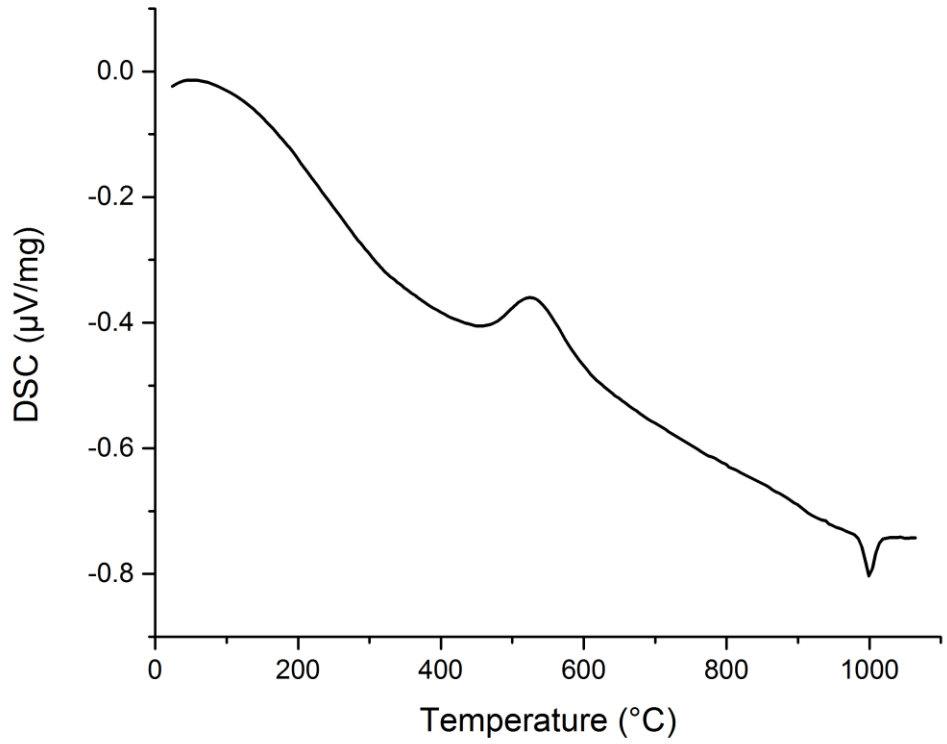

Figure 4: DSC Curve of Kaolinite Sample

3.2.2 Characterization of Textural Properties

Nitrogen adsorption isotherms were taken to measure the effect of kaolinite binder and pelletization pressure on the textural properties of UiO-66**.** Results from Figure 5 show the nitrogen isotherms for UiO-66_K650_20wt% not pressed and pressed at 6802 psi, 10689 psi and 17491 psi (UiO-66_K650_20wt% _no pressure, UiO-66_K650_20wt%_6802 psi, UiO-66_K650_20wt%_10689 psi and UiO-66_K650_20wt%_17491 psi respectively)

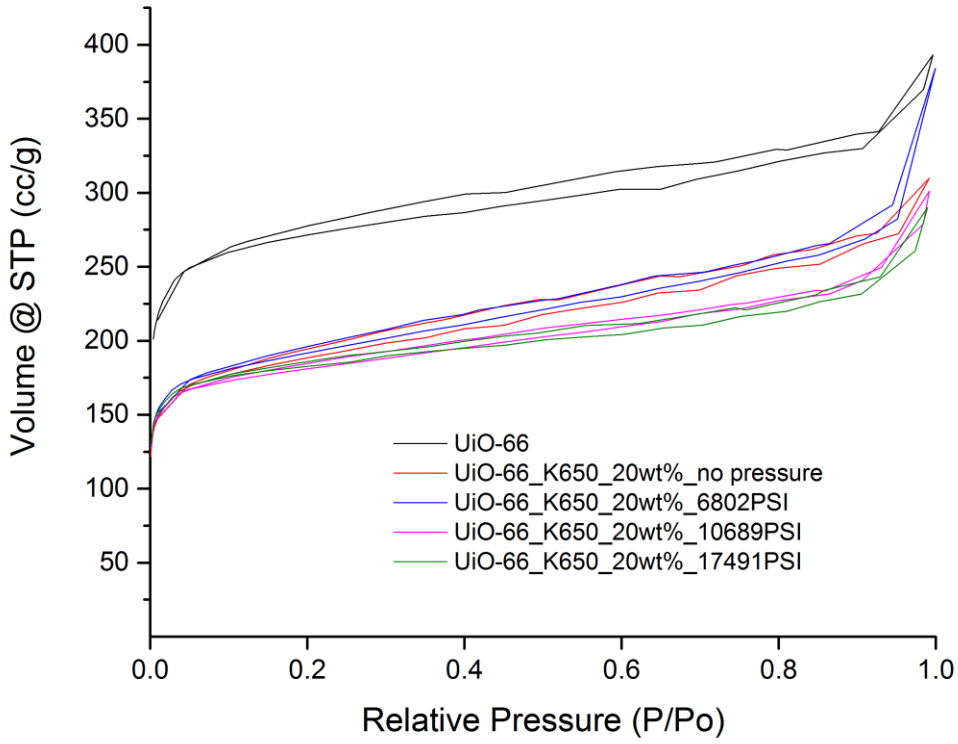

Figure 5: Nitrogen Isotherm Data Illustrating the Effect of Pelletization Pressure of Kaolinite Binder on the Uptake of UiO-66-S1

Nitrogen uptake significantly decreases when kaolinite is added, probably due to partial pore blocking. This analysis is further confirmed by a similar decrease in surface area and pore volume listed in Table 4. The change in nitrogen uptake between the pressed samples is quite insignificant when compared to the change in uptake that occurs between the UiO-66-S1 and the UiO-66-S1_kaolinite samples indicating the little effect pressure has on the overall gas uptake. The effect of the initial treatment temperature on the kaolinite binder is shown in Figure 6. The increase in temperature from 650 to 800 ^{o}C slightly decreases the nitrogen uptake of the adsorbent samples. At higher calcination

temperatures, the rate of decomposition of kaolinite increases. This increase in decomposition rate during thermal pre-treatment of kaolinite leads to the introduction of more unwanted materials and ions. During calcination of pellets at 200^{o}C, after the addition of the MOF, these unwanted substances fill up some of the pores of the MOF sample hence reducing its porosity and consequently its nitrogen uptake.

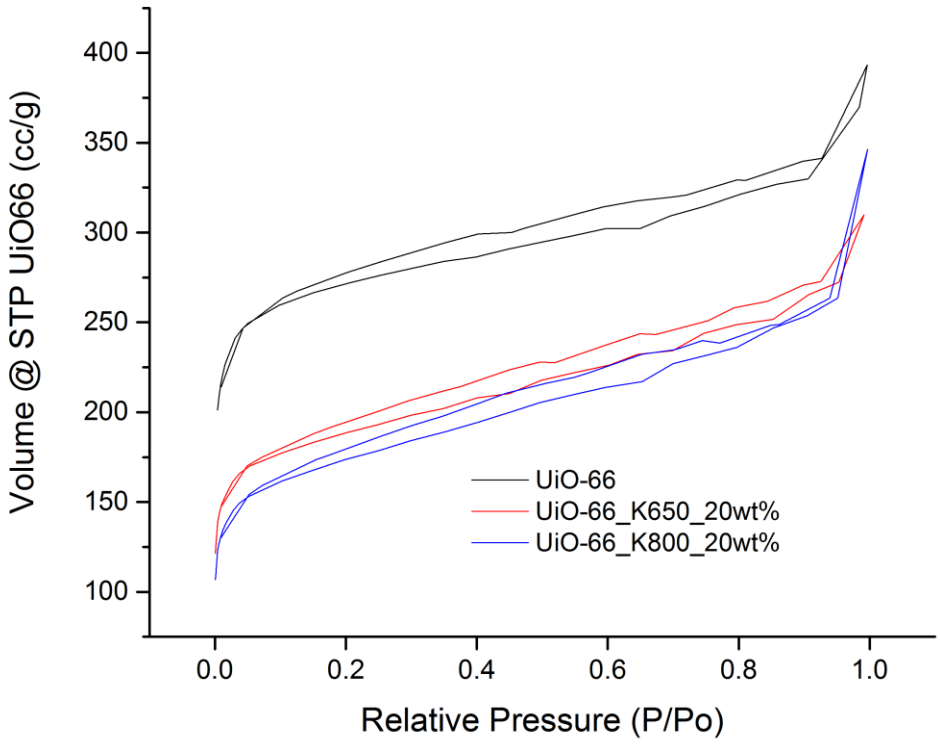

Figure 6: Nitrogen Isotherm Data Illustrating the Effect of Calcination Temperature of Kaolinite Binder on the Uptake of UiO-66-S1

Table 4. Textural Properties of UiO-66-S1 with Kaolinite Pre-Treated at 650 ^{o}C and 800 ^{o}C

	Surface Area (m^2/g)		Pore Volume (cc/g)	
UiO-66-S1	1033.		0.77	
	UiO-66_K650C_20wt%		UiO-66_K800C_20wt%	
Pelletization Pressure	Effective Surface Area (m^2/g UiO-66)	Effective Pore Volume (cc/g)_	Effective Surface Area (m^2/g)	Effective Pore Volume (cc/g)_
No pressure	878	0.56	794	0.67
6802 psi	904	0.74	898	0.63
10689 psi	874	0.58	816	0.57
17491 psi	890	0.50	846	0.58

3.2.3 Characterization of Physical Properties

3.2.3.1 Structural Stability Investigations

In other to determine the effect of kaolinite binder on the structural form of UiO-66-S1, powder XRD patterns were collected on UiO-66_K650_20wt% _no pressure, UiO-66_K650_20wt%_6802 psi, UiO-66_K650_20wt%_10689 psi and UiO-66_K650_20wt%_17491 psi. Due to the large size of the pellets (13mm diameter), the pellets were first crushed into small particles using a ceramic mortar and pestle to allow for easy characterization. Figure 7 shows a comparison between the as synthesized UiO-66, UiO-66_K650_20wt% and the pressed UiO-66_K650_20wt% samples. The peak at the 2θ value of 12^{o} was not pronounced in the simulated UiO-66 structure however it has been spotted in some experimental studies [37, 38]. Based on the uniformity in peak positions and the full width at half maximum (FWHM) peak width, it can be concluded that there is no significant structural degradation when the kaolinite binder was used even after been pressed at high pressures.

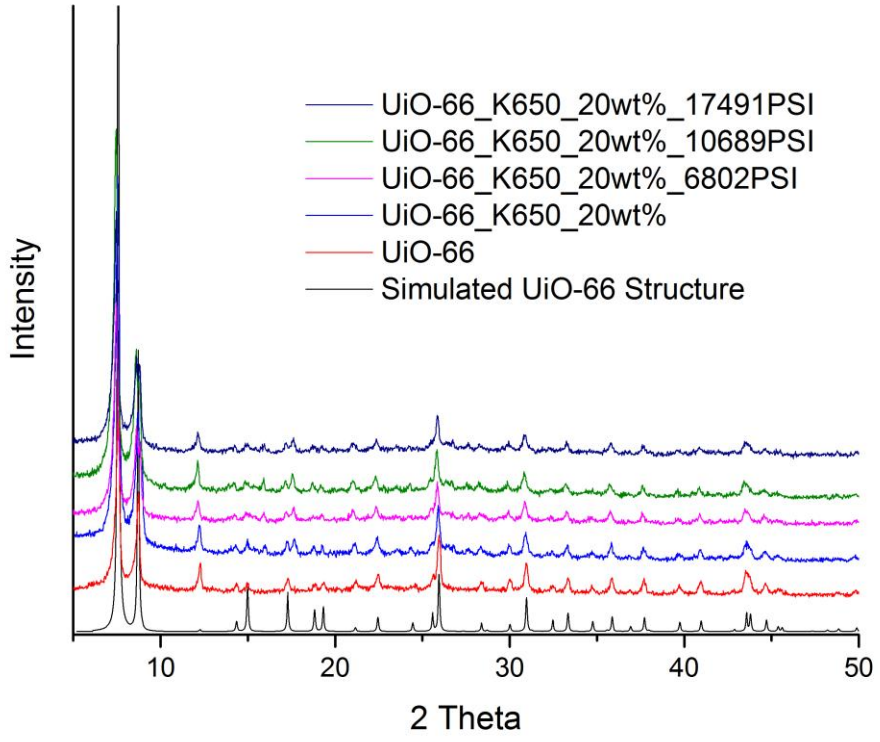

Figure 7: PXRD Patterns for UiO66 and Calcined UiO-66/Kaolinite Samples Pelletized at Different Pressures.

3.2.3.2 Investigation of Bulk Crush Strength

Kaolinite had shown to greatly improve the crush strength of zeolite pellets and this strength is well known to be even greater when pellets comprised of zeolite and kaolinite are calcined at higher temperatures [14, 39, 40]. Inspired by such increase in mechanical strength with kaolinite, crush strength investigations were carried out on UiO-66-S1 using kaolinite as a binder. Pellets comprised of the MOF alone were not dried or calcined since they were not mixed with any solvent prior to pelletizing while

pellets comprising of UiO-66-S1 and 20wt% Kaolinite pre-treated at 800 ^{o}C were calcined at 200 ^{o}C. Figure 8 below shows the effect of the 20 wt% kaolinite binder on the bulk crush strength of the UiO-66-S1 sample.

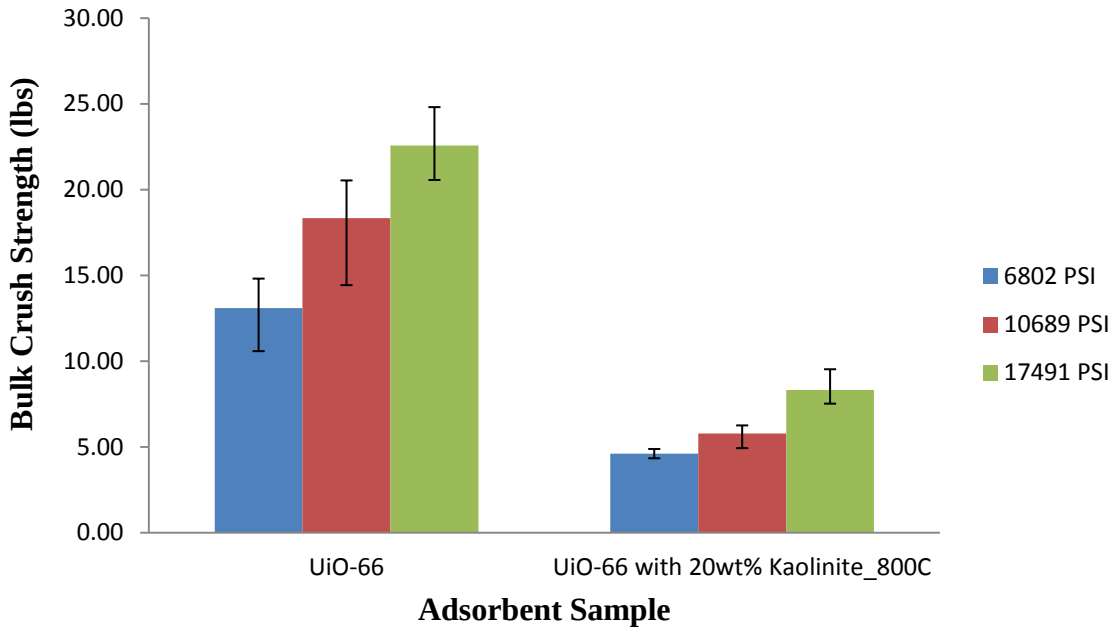

Figure 8: Effect of Kaolin on the Bulk Crush Strength of UiO-66-S1

Surprisingly, the crush strength of the pellets decreased appreciably when kaolinite was added. Since the kaolinite samples were thermally treated before they were mixed with the MOF sample, the decrease in crush strength with kaolinite most likely results from the poor interactions between the MOF and the calcined binder. With zeolites, an increase in crush strength is made possible by mixing the adsorbent sample with the binder before treatment at high temperatures. The results shown above indicate that even though the kaolinite binder had no effect on the crystal structure it reduces the mechanical strength of the MOF pellets. There is thus a need to investigate other binders.

3.3 Studies with Other Binders

3.3.1 Thermal Analysis of Polyvinyl Alcohol (PVA) and Tartaric Acid (TA)

Thermal degradation has an important effect on the mechanical strength of polymer–adsorbent composites. Baklouti et al.[41] examined the effect of PVA binder burnout on the mechanical strength of green alumina samples and observed significant variations in the mechanical strength during thermal debinding. The strength was initially found to increase steadily when calcined up to the melting point of the polymer. It then decreased gradually until the final decomposition temperature of the binder (~600 ^{o}C) was reached and then increased steadily again above 800 ^{o}C due to the formation of grain boundaries. Taking into consideration the thermal stability of the as-synthesized UiO-66 sample, experiments were only conducted to the melting point of the PVA sample.

TG and DSC analysis were performed to determine the decomposition temperature and melting point of PVA. The fully hydrolyzed PVA binder used has a higher decomposition rate so water is eliminated from the hydroxyl groups at lower temperatures. From the TG curve in Figure 9, PVA starts decomposing at about 140^{o}C. This temperature is much lower than the melting point temperature, which occurs at about 220 ^{o}C (DSC curve, data not shown). From these results, temperatures of 140 ^{o}C

and 190 ^{o}C were chosen to investigate the effect of .binder temperature on the MOF.

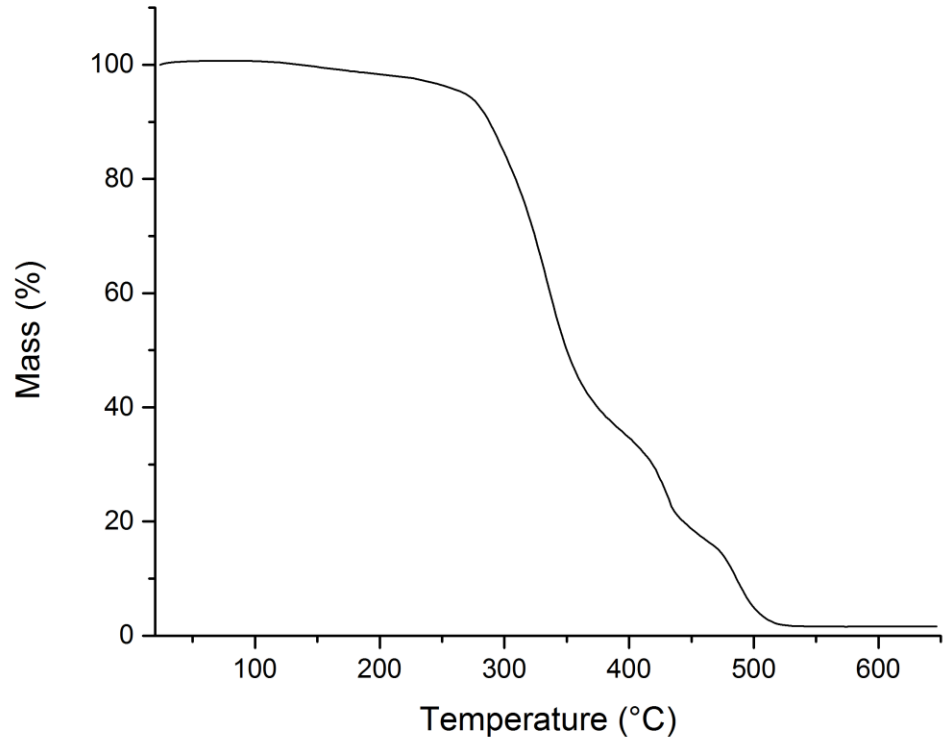

Figure 9: TGA Curve for Polyvinyl Alcohol (PVA)

With tartaric acid, thermolysis was carried out at 10 ^{o}C/min from 30 ^{o}C to 550 ^{o}C under flowing air. As shown in Figure 10, the first endothermic peak from the DSC curve relates to the melting point temperature of 222 ^{o}C. This is about the same temperature when tartaric acid begins to decompose (TG curve). To avoid weight losses of tartaric acid at 222 ^{o}C, 140 ^{o}C was chosen as the desired temperature to investigate the effect of the binder temperature on the MOF.

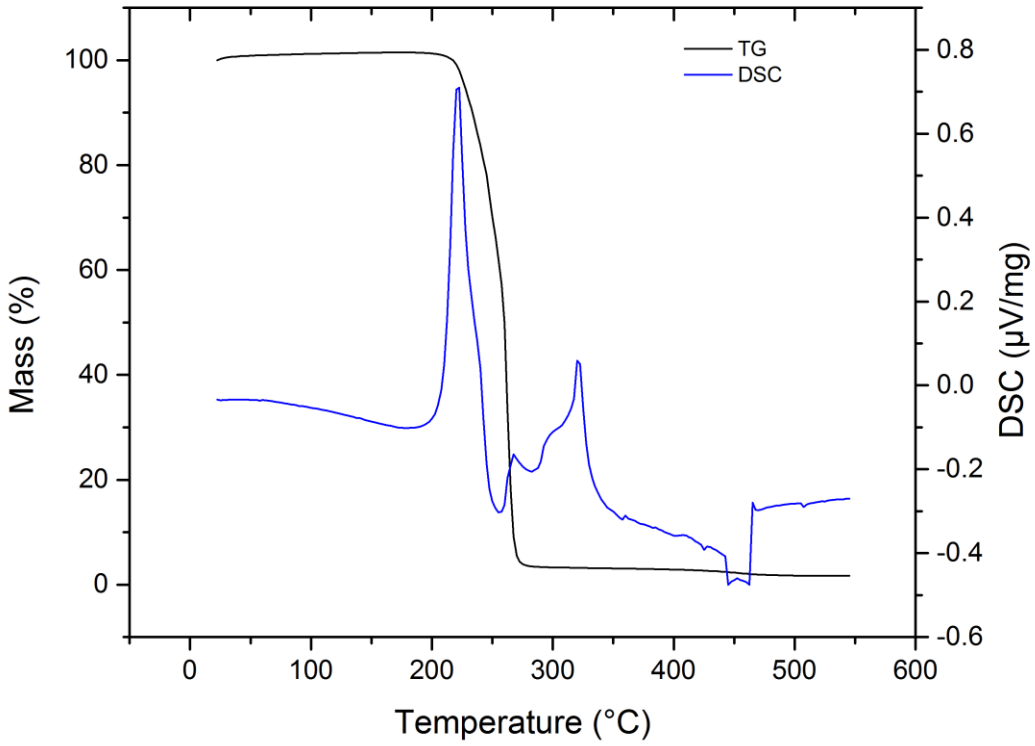

Figure 10: TGA and DSC Curves for Tartaric Acid.

3.3.2 Characterization of Physical Properties

3.3.2.1 Structural Stability investigations

UIO-66-S1_PVA_13wt% and UIO-66-S2_TA_13wt% were pressed at 6802, 10689 and 17491 psi. Table 5 shows the names assigned to the corresponding pellets for the remainder of this work.

Table. 5 Designated Names for PVA and TA Pellets Pressed at 6802, 10689 and 17491 psi. Designated names for pressed samples are in bold

Pressure	UIO-66-S1_PVA_13wt%	UIO-66-S2_TA_13wt%
6802 PSI	**UIO-66-S1_PVA_13wt%_6802PSI**	**UIO-66-S2_TA_13wt%_17491PSI**
10689 PSI	**UIO-66-S1_PVA_13wt%_10689PSI**	**UIO-66-S2_TA_13wt%_10689PSI**
17491 PSI	**UIO-66-S1_PVA_13wt%_17491PSI**	**UIO-66-S2_TA_13wt%_17491PSI**

Figures 11 and 12 show the effect of PVA and tartaric acid respectively on UiO-66-S2. Powder XRD patterns collected for the PVA treated MOF samples indicate that pelletization pressure up to 17491 psi has no significant effect on the crystal structure of the original MOF sample. Powder XRD patterns were also generated for UiO-66-S2_PVA samples uncalcined and calcined at 190 and 200 ^{o}C (UiO66-S2_PVA_UC, UiO66-S2_PVA_190C and UiO66-S2_PVA_200C respectively) to investigate the effect of high thermal treatment on the crystal structure of the MOF. The pellets obtained from such treatment were observed to change color from white to brown as shown in Figure 13. However pXRD patterns obtained (Figure 14) indicate no significant change in crystal structure between the uncalcined and calcined pellets.

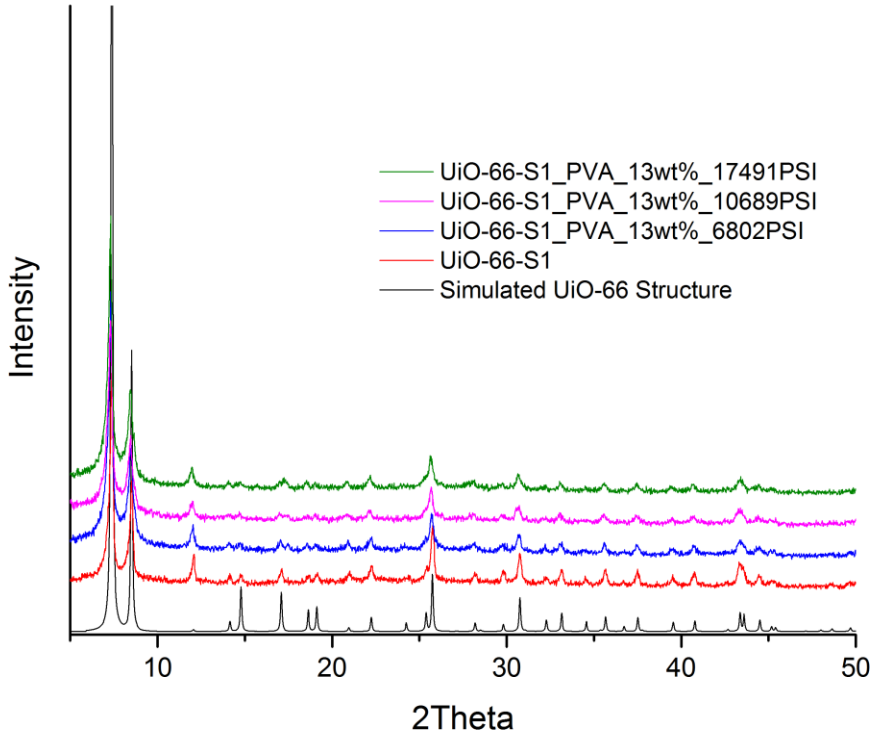

Figure 11: PXRD Patterns Illustrating the Effect of Pressure on UiO-66-PVA Samples.

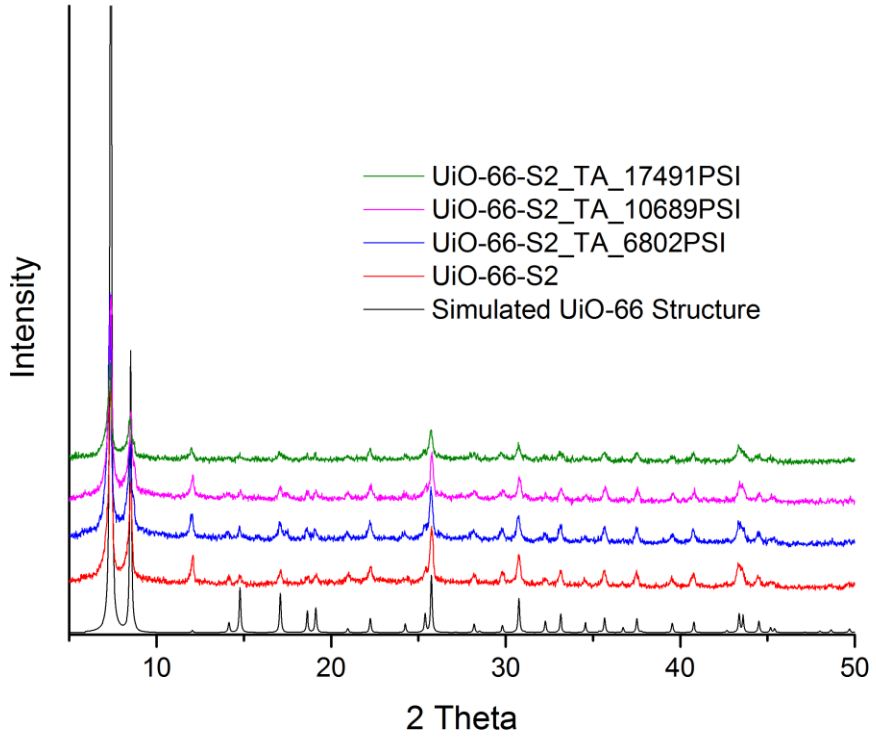

Figure 12: PXRD Patterns Illustrating the Effect of Pressure on UiO-66-Tartaric Acid Samples.

Figure 13: UiO-66/PVA Pellets Calcined at Different Temperatures. (a) Pellets not calcined. (b) Pellet Calcined at 140^{o}C. (c) Pellet Calcined at 190^{o}C. Each pellet is a disc of ~ 13 mm in diameter.

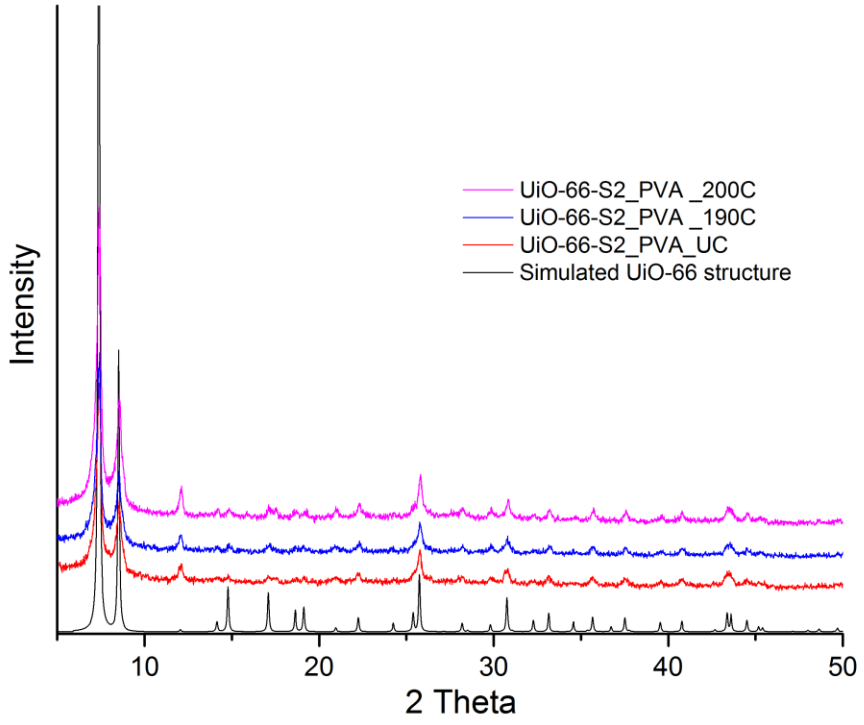

Figure 14: PXRD Patterns Illustrating the Effect of Calcination Temperature on UiO-66-S2_PVA Samples.

3.3.2.2 Investigation of Bulk Crush Strength

3.3.2.2.1 Effect of Binder Composition on Bulk Crush Strength

As expected from Figure 15, the crush strength increased as applied pressure increased. Pellets that were not calcined were still first dried at 100^{o}C before further tests for crush strength. Water, which was used as plasticizer, allows for proper diffusion and agglomeration of the polymer but decreases the strength of the compacts and thus had to be first eliminated to improve the mechanical strength of the pellets.

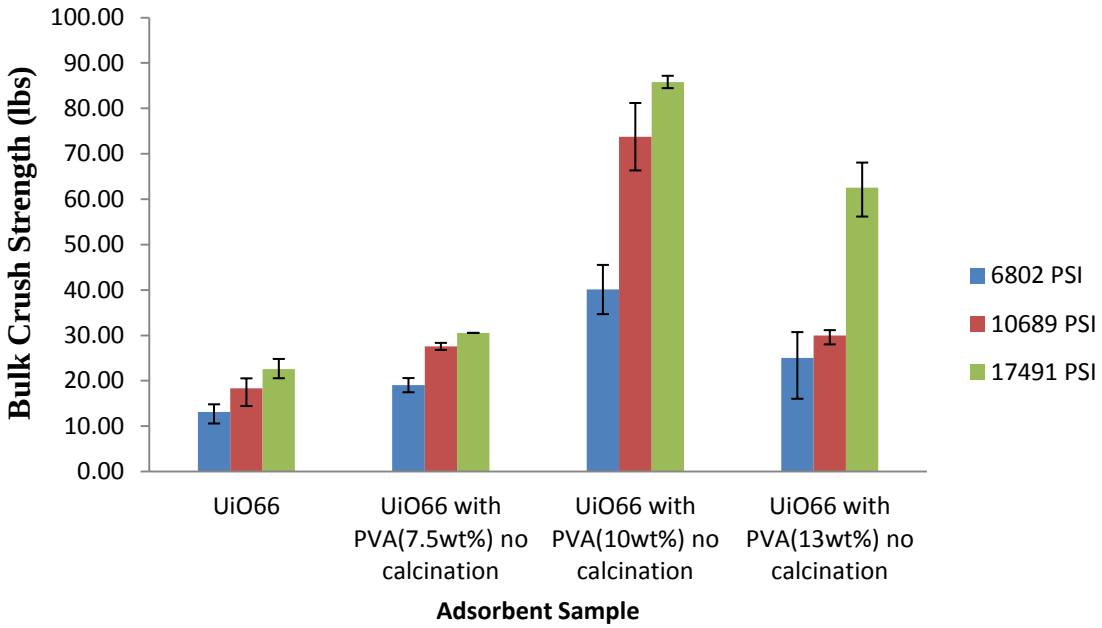

Figure 15: Effect of PVA composition on the Bulk Crush Strength of UiO-66-S1

The bulk crush strength of the formed final pellets was also studied with respect to the binder composition. From Figure 15, it can be seen that the strength of the uncalcined pellets increases to a maximum when 10wt% PVA binder was applied and then decreases afterwards. This was unexpected as it was thought that an increase in binder content should continuously increase the strength of the pellets. This observation instigated the determination of the crush strength of the polymer alone in order to determine how strong the interactions within the polymer were compared to those of the as-synthesized MOF sample.

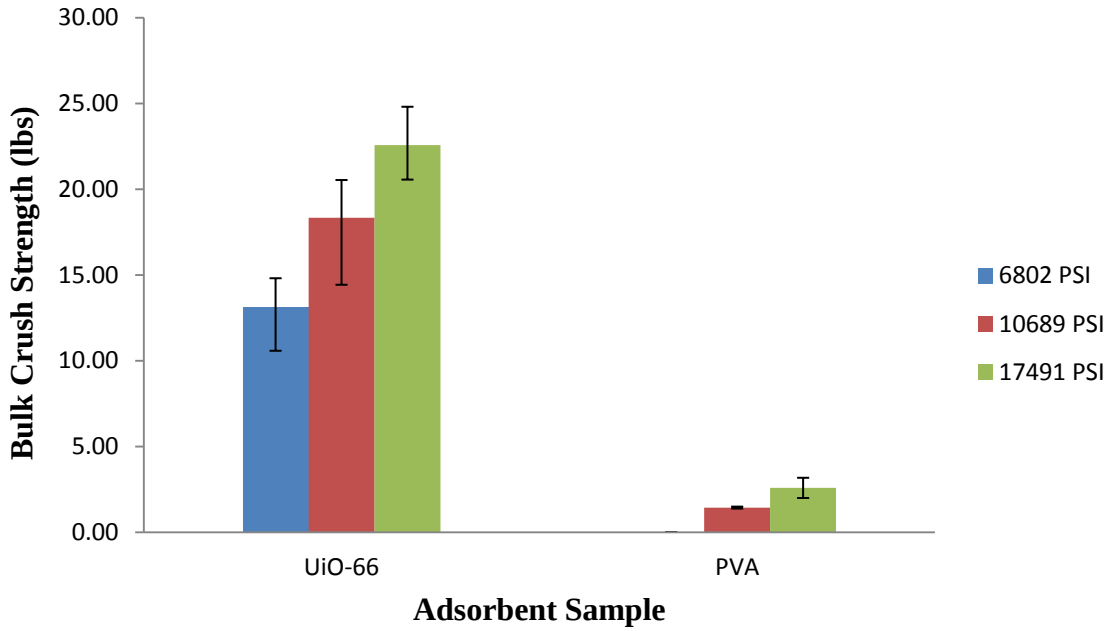

Figure 16: Comparison between Bulk Crush Strengths of UiO-66-S1 and PVA Pellets

(a) (b) (c)

Figure 17: PVA pellets pressed at (a) 6802 psi (b) 10689 psi (c) 17491 psi

Figure 16 shows the comparison between crush strengths of UiO-66 and PVA. The crush strengths of PVA pellets pressed at 6802 psi could not be measured because of the inability to form well-defined disc shaped pellets (Figure 17) at such low pressure.

Our data indicate that the strength of the compact is controlled by three interactions, namely the MOF-MOF, MOF-PVA and PVA-PVA interactions. For low PVA content, the MOF-PVA interactions dominates, leading to higher crush strength. However as the PVA content increases to 13wt%, the smaller PVA-PVA interactions eventually dominate leading to reduced crush strength seen in Figure 15. This dominance in PVA–PVA interactions is however not sufficient enough to reduce the crush strengths of the UiO66-S2_PVA_13wt% pellets further than those of pellets comprised of only the MOF. A reason for this is due to the lower amount of some strong MOF-PVA interactions still present in pellets made with 13wt% PVA

3.3.2.2.2 Effect of Calcination Temperature on Bulk Crush Strength

Figure 18 shows the effects of calcination temperature on the bulk crush strength of different pellets. As earlier shown from the TGA result in Figure 9, decomposition of PVA starts at about 140 ^{o}C. The small weight loss in PVA content during the initial decomposition is associated with a slight reduction in crush strength. At 190 ^{o}C however, which is almost at its melting point temperature of 222 ^{o}C, the decomposition of PVA is more rapid and this leads to a more significant reduction in crush strength. Similar results were obtained for other binder compositions. For the calcination process of the MOFs treated with 10wt% PVA, there was an observed inconsistency in the ramp rate of the furnace. The intended temperatures of 140 and 190 ^{o}C overshot to 175 ^{o}C and 208 ^{o}C respectively for about ten minutes before going down back to their set temperatures. Figure 19 compares the effects of PVA and tartaric acid binders on the strength of the MOF pellets under various conditions. From the results we can clearly see that the use of PVA offers the highest strength of the formed pellets.

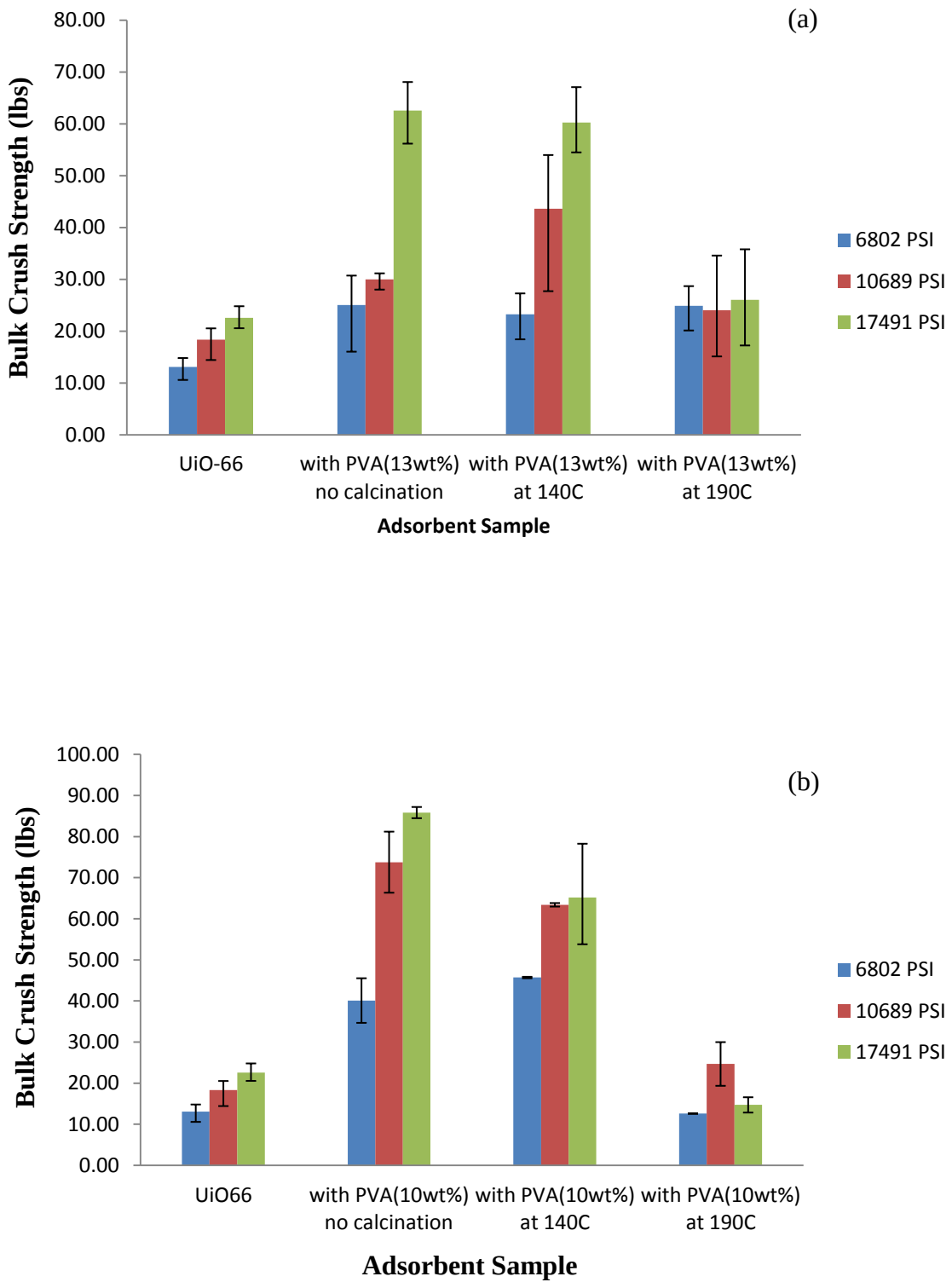

Figure 18: Bulk Crush Strengths of UiO-66-S2_PVA Pellets Calcined at Different Temperatures. (a) Pellets Comprised of UiO-66-S1 and 13wt% PVA. (b) Pellets Comprised of UiO-66-S2 and 10wt% PVA.

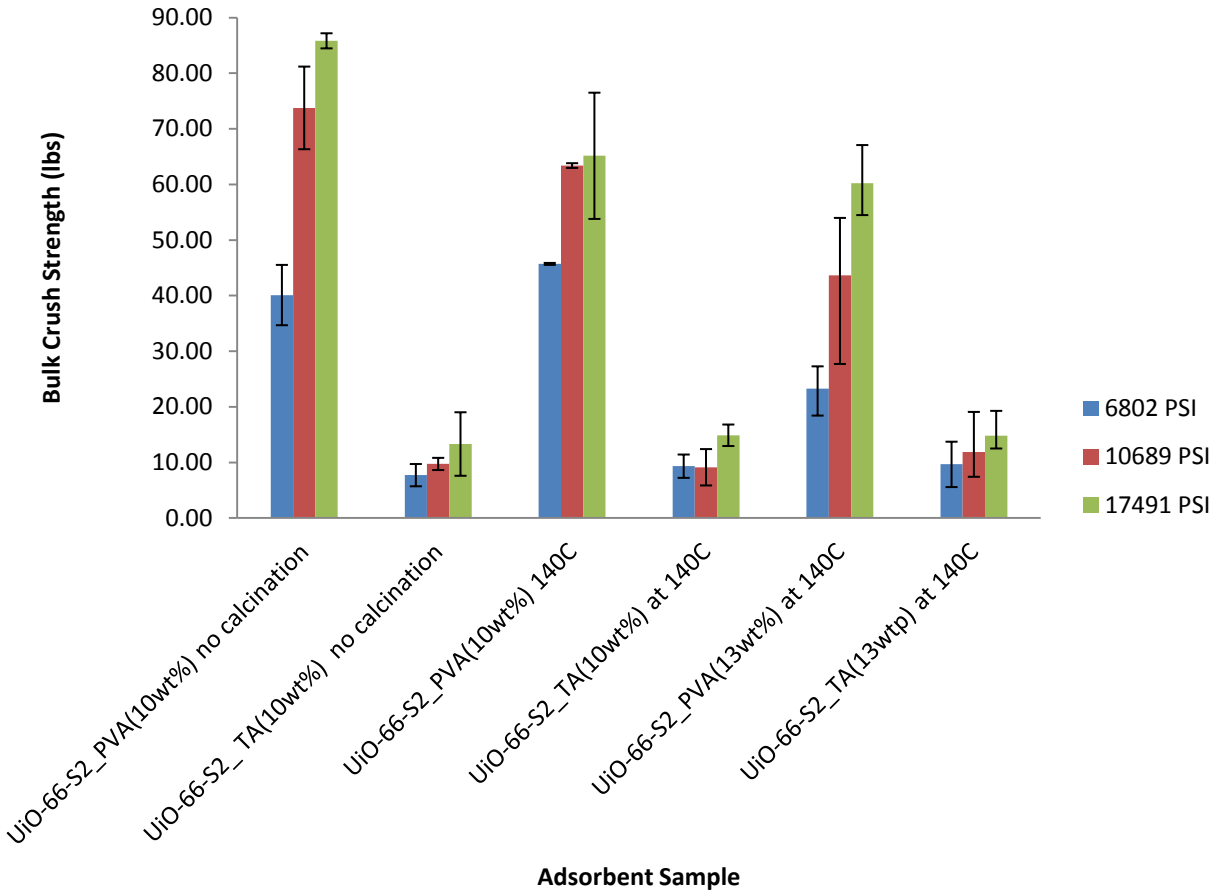

Figure 19: Comparison of Different Binder Conditions on the Bulk Crush Strength of UiO-66 Pellets

3.3.2.3 Bulk Density Investigations

Density measurements were made on the all pellets made with different binders. Prior to recording density measurements for pellets, the density of the as-synthesized powdered UiO-66 sample was measured to be 0.31g/cc. This value is much smaller than the skeleton density of the UiO-66 crystal structure recorded (1.23g/cc)[42]. The lower density of the as-synthesized powder is probably due to the extra dead volume present between crystals in their loose state. In almost all cases an increase in binder content

leads to an increase in bulk density. A reduction in density can however be observed for the uncalcined pellets prepared with PVA 13wt%. This trend is quite similar to that of the crush strength measurements discussed previously for the same sample, most likely due to the increase in the weak PVA-PVA interactions. As calcination temperature increases in the decomposition range of the binder, lower density values were recorded. Again these results are consistent with similar trends in the crush strengths.

Table 6. Bulk Density Measurements for Various UiO-66-PVA Pellets Conditions

Temperature	Binder Used	Density (g/cc)		
		6802 PSI	10689 PSI	17491 PSI
No Calcination	PVA 7.5wt%	0.88	0.99	1.02
	PVA 10wt%	0.93	1.05	1.12
	PVA 13wt%	0.91	0.97	1.04
140 ^{o}C	PVA 10wt%	0.91	1.01	1.08
	PVA 13wt%	0.98	1.05	1.04
190 ^{o}C	PVA 10wt%	0.75	0.84	0.89
	PVA 13wt%	0.98	0.97	0.95

Table 7. Bulk Density Measurements for Various UiO-66-Tartaric Acid Pellets Conditions

Temperature	Binder Used	Density (g/cc)		
		6802 PSI	10689 PSI	17491 PSI
No Calcination	Tartaric Acid 10wt%	0.91	1.01	1.15
	Tartaric Acid 7.5wt%	0.81	1.07	1.08
140^{o}C	Tartaric Acid 10wt%	0.94	0.97	1.11

3.3.3 Adsorption Tests

3.3.3.1 Nitrogen Isotherm Measurements

The porous structure of UiO-66 when treated with PVA and tartaric acid was tested by nitrogen adsorption and the results are shown in Tables 8 and 9. The effective surface area of the MOF in each sample was determined by normalizing out the binder present with respect to the composition of MOF present and was seen to be smaller with the bulkier tartaric acid than with PVA. The surface area and pore volume of binder-treated MOFs reduces significantly due to the reduction in porosity accessible to nitrogen caused by the partial pore filling with the binders as seen from Figure 20. This trend was similar to the results obtained during CO_2 adsorption measurements that will be later

discussed. As expected, increasing the amount of binder content as shown in Tables 8 and 9 reduces the surface area and total pore volume of the MOF sample.

Table 8. Textural Properties of UiO-66 with Different Compositions of PVA

Sample	Pressure (psi)	Surface Area (m^2/g)	Effective Surface Area (m^2/g UiO66)	Effective Total Pore Volume (cc/g UiO66)	% Micropore Volume
UiO-66-S2_PVA7.5wt%	6802	1029	1112	0.86	60.0
	10689	989	1069	0.70	67.5
	17491	825	892	0.62	68.8
UiO-66-S2_PVA10wt%	6802	825	917	0.53	76.9
	10689	904	1004	0.67	69.1
	17491	894	993	0.66	70.4
UiO-66-S1_PVA13wt%	6802	663	762	0.53	70.1
	10689	811	932	0.68	65.9
	17491	815	936	0.67	66.4

Table 9. Textural Properties of UiO-66 with Tartaric Acid as a Binder

Sample	Pressure (psi)	Surface Area (m^2/g)	Effective Surface Area (m^2/g UiO-66)	Effective Total Pore Volume (cc/g)	% Micropore Volume
UiO-66-S2_Tartaric acid10wt%	6802	727	808	0.58	66.5
	10689	625	694	0.54	62.0
	17491	527	586	0.44	64.1

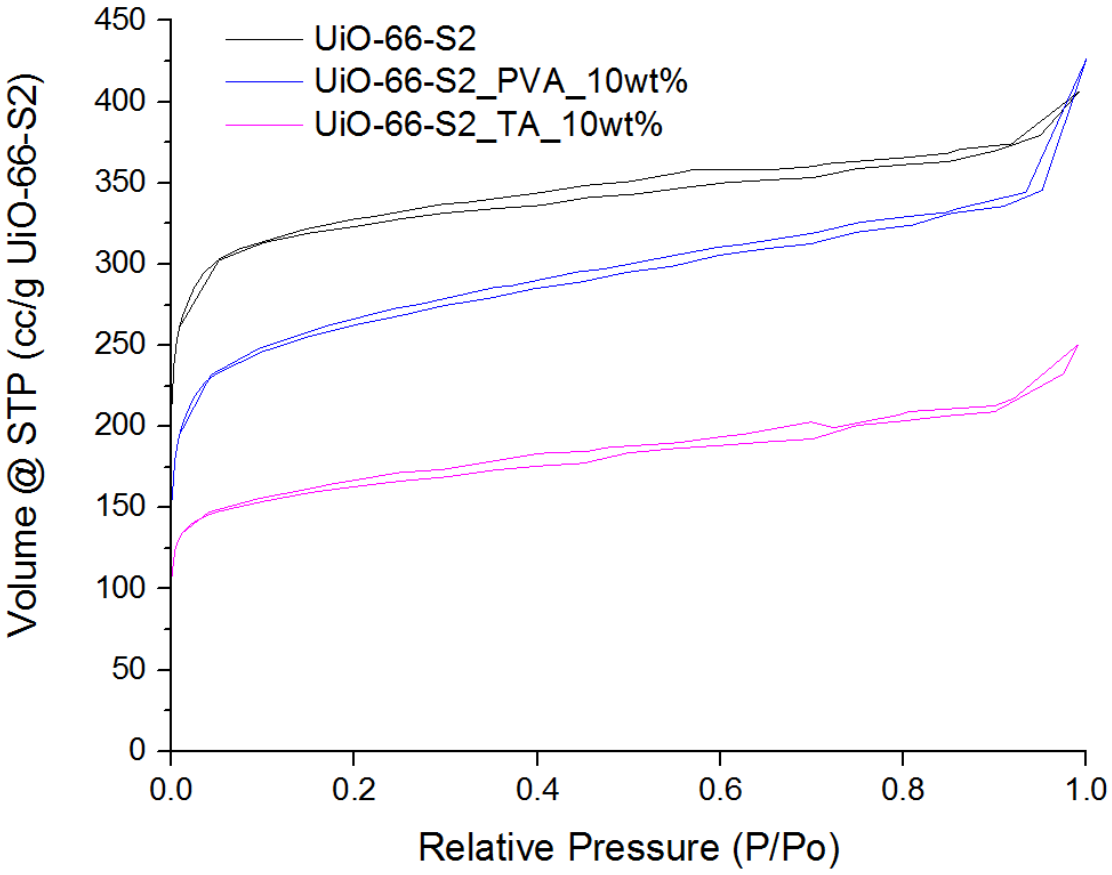

Figure 20: Nitrogen Isotherm Data Illustrating the Effect of Binder on the Uptake of UiO-66-S2

3.3.3.2 CO_2 Adsorption in UiO-66

Results from Tables 3, 8 and 9 indicate that the addition of binders decreases the effective surface area and pore volume of the MOF. Generally adsorbents with lower surface areas and pore volume tend to adsorb less CO_2. Application of these materials as useful adsorbents for CO_2 capture requires a reasonable adsorption capacity. Adsorption isotherms were thus measured to examine the adsorption capacity for CO_2 with the different materials. Due to the different composition of binders present within each

material, the net adsorption capacity was measured to effectively compare the gas uptake at low and high pressure amongst all materials. The number of mmoles of gas adsorbed per unit gram of MOF present was thus measured by normalizing out the binder composition.

The CO_2 adsorption isotherms for the as-synthesized UiO-66 samples and the UiO-66 samples pressed at different pressures as shown in Figure 21 exhibit type I isotherms with no hysteresis. The adsorption isotherms for the as-synthesized UiO-66-S1 and UiO-66-S2 present high uptakes of 6.83 and 6.69 mmol/g respectively at 15 bar which is slightly higher than that recorded by Wiersum et al.[43]. The effect of pressure on the as-synthesized MOF sample is quite significant as a 24.6 % decrease in CO_2 adsorption was observed at 6802 psi. The collapse in the pore structure as evident by the reduction in micropore volume (17.0 %) at 6802 psi might be a possible reason for this sharp decrease in CO_2 adsorption capacity. As the applied pressure was increased to 17491 psi, the reduction in CO_2 uptake became less drastic because of the gradual decrease in the collapse of the micropore structure within all pressed samples as seen from the micropore volumes in Table 3.

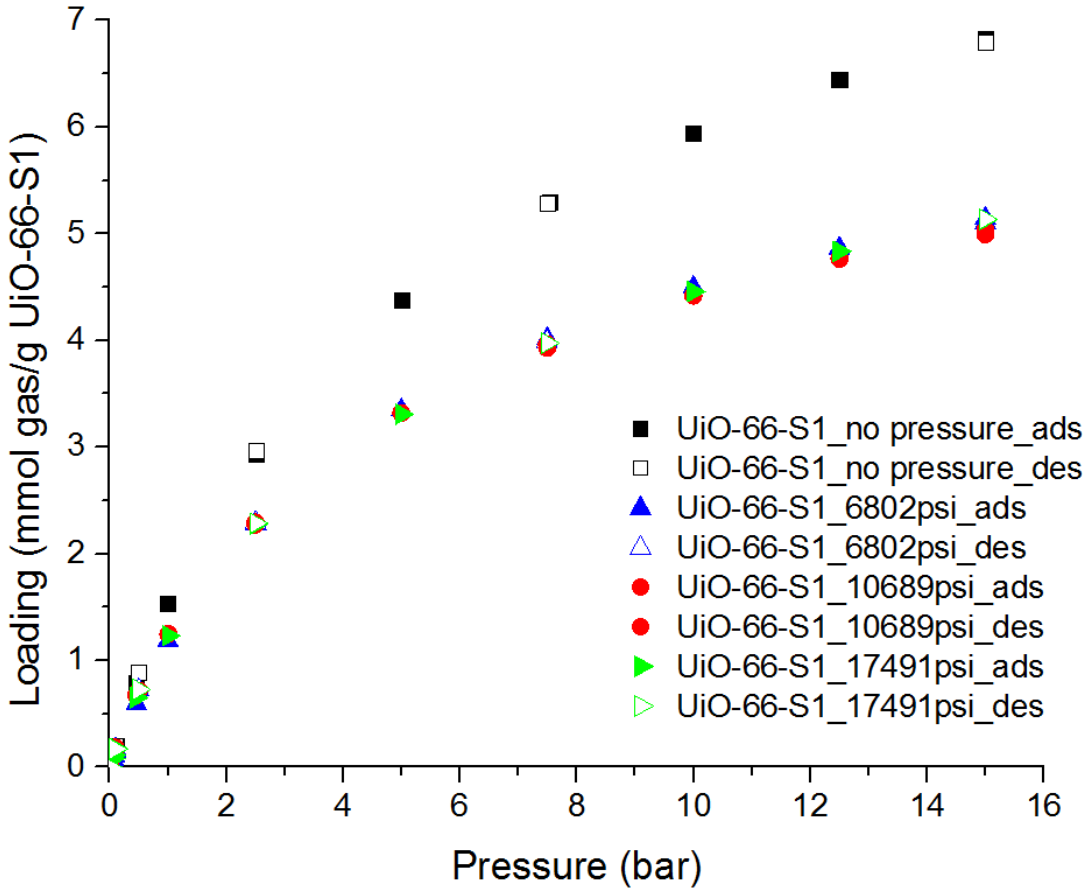

Figure 21: Adsorption-Desorption Isotherms for CO_2 at 298 K for the Parent and Pressed UiO-66-S1 Samples.

3.3.3.3 CO_2 Adsorption in UiO-66/Binder Mixture

Low and high CO_2 adsorption isotherms were collected for compacts prepared with different binders. From Figure 22 it can be concluded that at high pressures the highest gas uptake with binders was achieved when PVA was used as a binder. At low pressures (Figure 23), the amount of CO_2 adsorbed was higher with the PVA binder than the as-synthesized material. The polar hydroxyl functional group in PVA led to strong dispersive interactions and was responsible for increased adsorption at low pressures Although, the functional group of tartaric acid (two hydroxyl groups and two carboxyl

groups) accounted for a combined higher polarity, it is possible that due to its bulkiness, it occupied more pore space which led to lower CO_2 adsorption at even at low pressures At higher pressures, the strong binding sites became completed occupied and since the parent MOF material had a higher pore volume, its adsorption loadings became higher. Kaolinite is a bulky inorganic binder and offered no polar functionality which led to a much reduced CO_2 adsorption capacity at both low and high pressures. The high loadings obtained with the PVA treated MOF when activated at 220 ^{o}C, indicates that the change in form as observed by color change in Figure 13 had no detrimental effect on the absorption capacity of the material.

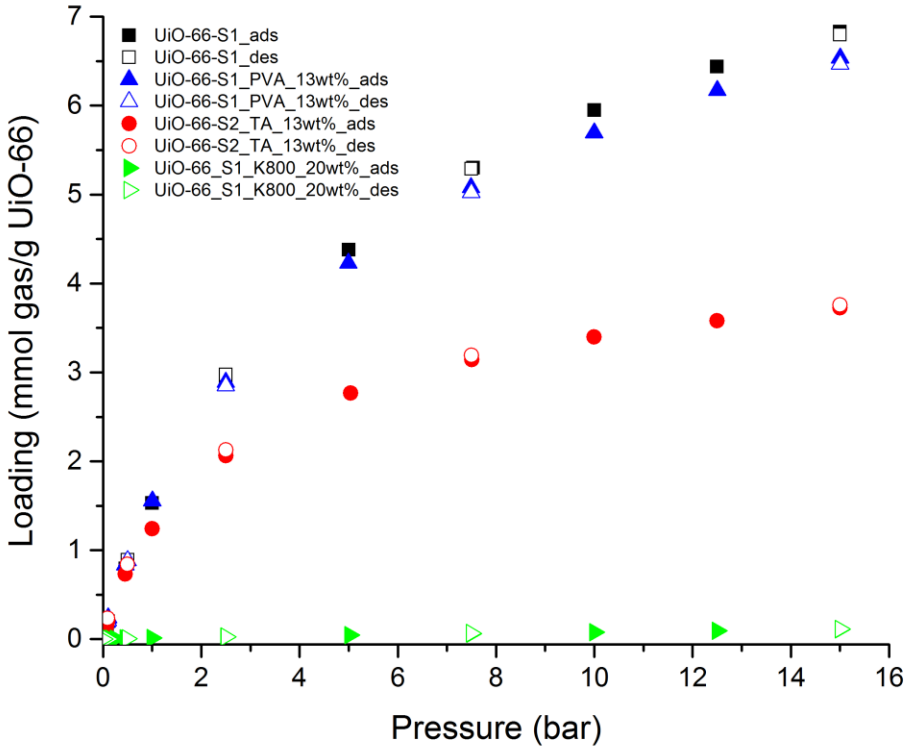

Figure 22: High Pressure Adsorption-Desorption Isotherms for CO_2 at 298 K for the UiO-66 and UiO-66 Mixed with Different Binders

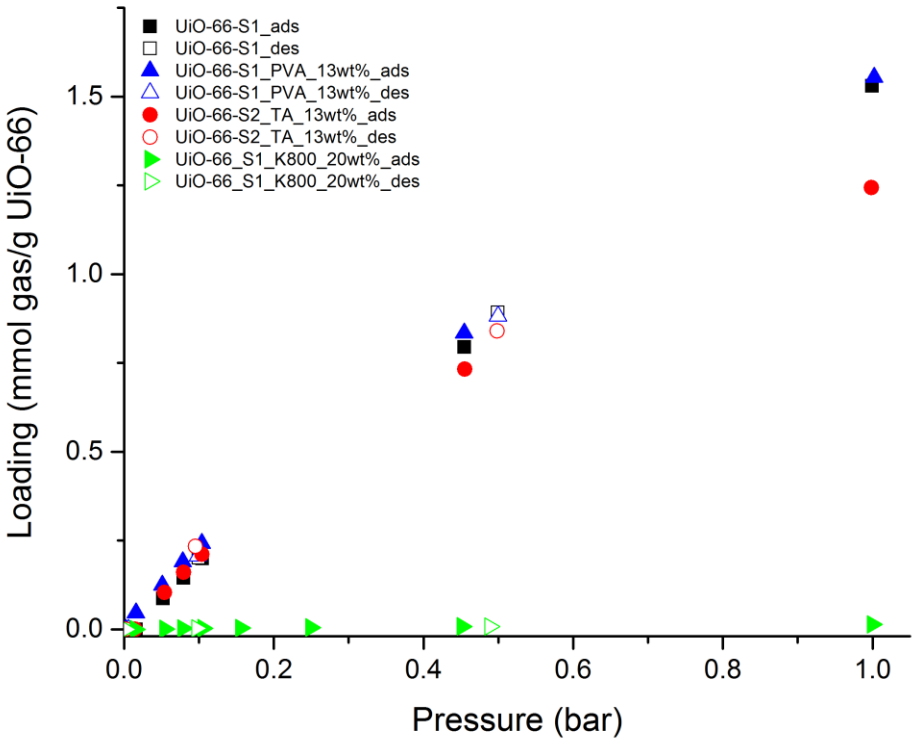

Figure 23: Low Pressure Adsorption-Desorption Isotherms for CO_2 at 298 K for the UiO-66 and UiO-66 Mixed with Different Binders

3.3.3.4 Effect of CO_2 Adsorption on UiO-66-PVA Pellets

Inspired by the high mechanical strength and relatively high CO_2 adsorption power exhibited by samples compacted with PVA, studies were also made to investigate the effect of pelletization pressure on the adsorption loadings of the UiO-66-PVA pellets. The CO_2 adsorption isotherms shown in Figure 24 display a similar trend of a significant decrease in loading between powder and pressed samples as for those pellets made with just the parent material. As earlier stated, this can be attributed to the crystal structure collapse during the pelletization process. However, a much lower reduction in loading

(9.6%) was observed between the powdered sample and the sample pressed at 6802psi. A reason for this could be that the PVA binder already contributes a significant amount of mesoporosity before pelletization as seen in Figures 25 and 26. Within the pressed samples, this change is not as significant as there is already a high degree of mesoporosity present.

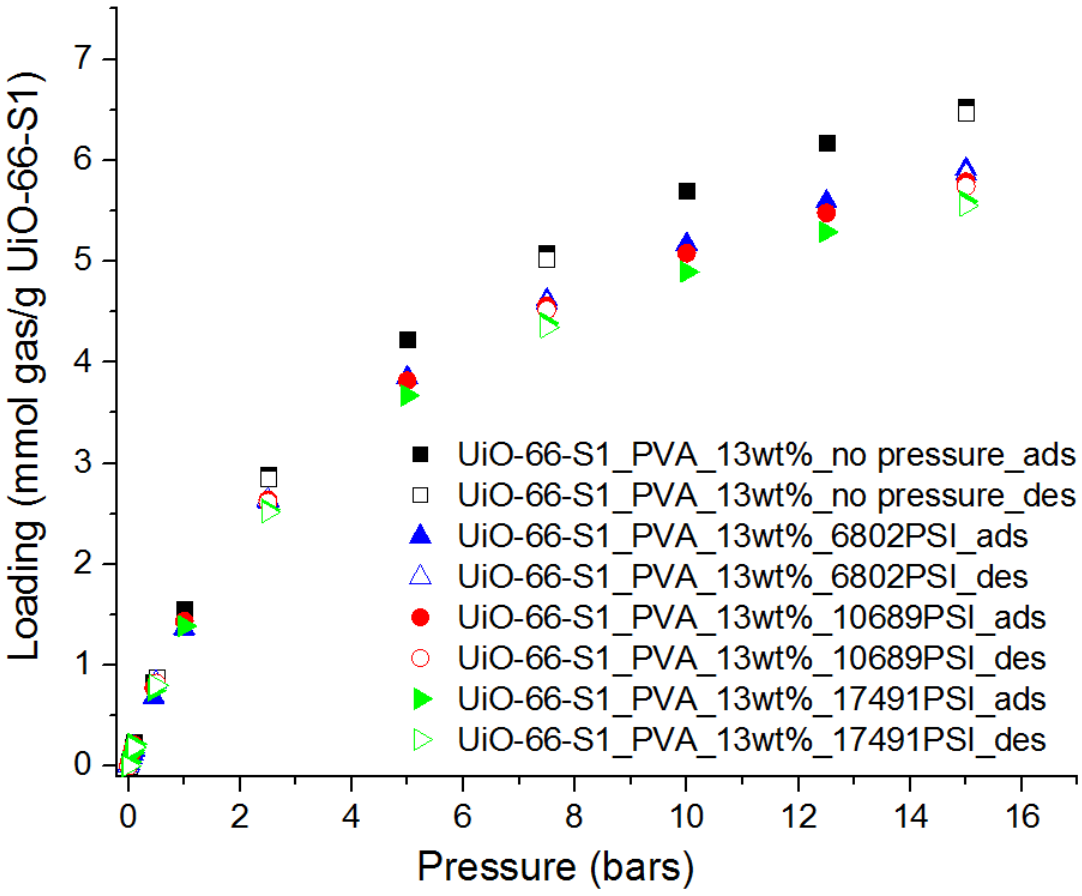

Figure 24: Adsorption-Desorption Isotherms for CO_2 at 298k from UiO-66-S1_PVA13wt% Samples.

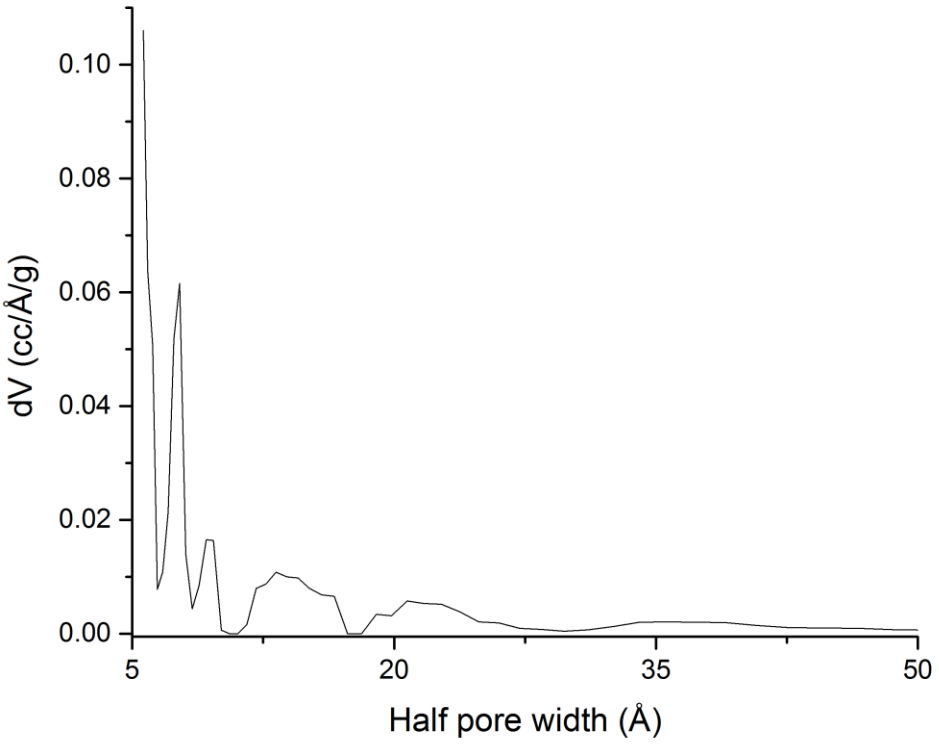

Figure 25: Pore Size Distributions for UiO-66-S1

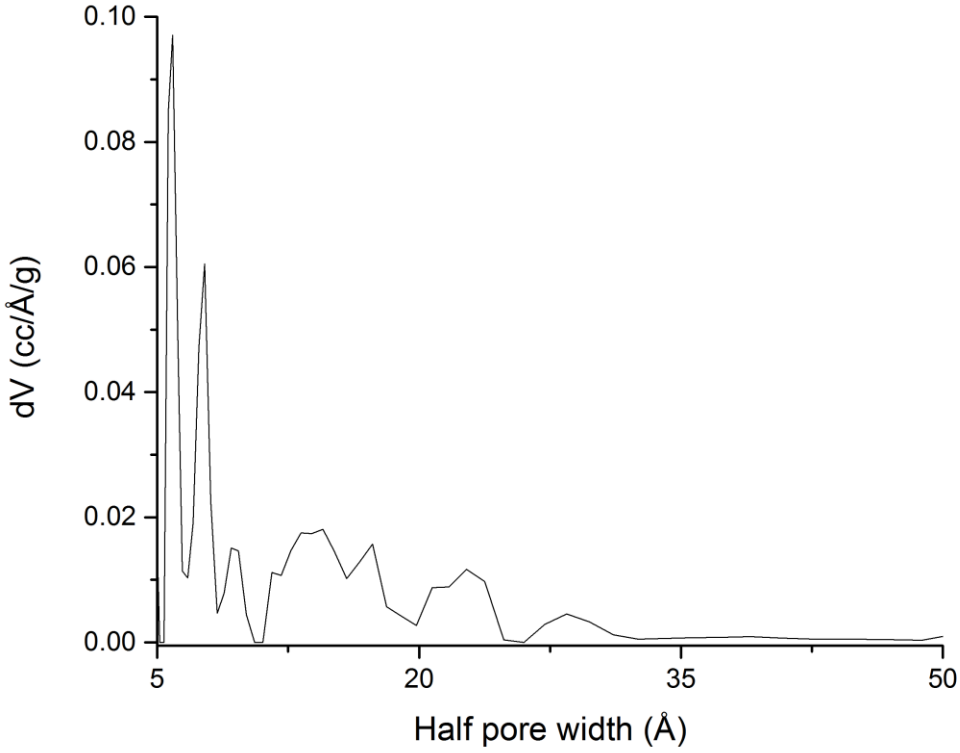

Figure 26: Pore Size Distributions for UiO-66-S1_PVA_13wt%

CHAPTER 4

CONCLUSIONS AND RECOMMENDATIONS FOR FUTURE WORK

4.1 Conclusions

Polyvinyl alcohol is seen as the most promising binder for improving the mechanical strength of the parent UiO-66 material due to the slight decrease in textural and adsorption properties and the quite significant increase in crush strength of the parent MOF material it offers. Contrary to what was initially hypothesized based on studies previously done with zeolites, an increase in calcination temperature and increase in the binder content does not always lead to an increase in the bulk crush strength of the composite. The presence of weak PVA-PVA interactions was found to become predominant as the binder content increased, which led to reduced crush strengths. The decomposition temperatures of the parent MOF and the binder are seen to be important parameters when considering making high quality pellets. Table 9 is a summary of results obtained from pellets that displayed an increase in crush strength. From results gathered from this study, a conclusion can be made that uncalcined UiO-66-PVA pellets pressed at 17491psi with a 10 wt% portion binder is a useful approach of forming quality pellets. These conditions give the best properties among the conditions tested as it resulted in a 29% decrease in surface area, a 6.3% decrease in adsorption power at maximum loading, a 5.9%decrease in total pore volume, a 261% increase in bulk density and a 280% increase in the bulk crush strength when compared with the standard properties of the as-

synthesized UiO-66 sample. Powder XRD patterns from all UiO-66-PVA samples also indicated that the MOF structure was not significantly affected.

Table 10. Comparison of Textural and Mechanical Properties for Various Binder Conditions

Binder Conditions	% Increase in bulk density from parent MOF	% Decrease in surface area from parent MOF	% Increase in bulk crush strength from parent MOF
PVA7.5wt%_17491psi	229	34.2	35.3
PVA7.5wt%_10689psi	219.4	21.1	22.1
PVA10wt%_17491psi	261.3	28.7	280.1
PVA10wt%_10689psi	238.7	27.9	226.7
PVA7.5wt%_6802psi	200.0	34.2	77.6
PVA10wt%_140^{o}C_17491psi	248.4	-	188.5
PVA10wt%_140^{o}C_10689psi	225.8	-	180.7
PVA10wt%_140^{o}C_6802psi	193.5	-	102.4
PVA13wt%_17491psi	235.8	35.8	177.1
PVA13wt%_140^{o}C_17491psi	235.5	21.1	166.8
PVA10wt%_140^{o}C_10689psi	238.7	21.5	93.2

Despite the significant decrease in surface area, this percentage is still less than those obtained for zeolite 5A with different binders. A series of tests have been

performed with zeolite 5A to determine the most appropriate set of conditions that produced the best crush strength while still maintaining a reasonable adsorption capacity. The recorded crush strength for zeolite 5A when treated with 15wt% kaolin binder at 550 ^{o}C was calculated to be 27.65 lb with an estimated 38% decrease in surface area[40]. With 7.5 wt% portion of tartaric acid the calculated crush strength for zeolite 5A was 46.31lbs with an estimated 53.2% decrease in surface area[40].

From all the results and comparisons made, we can see the potential of UiO-66 with PVA as a binder as a promising composite for future research on using MOFs in practical applications. However more studies must be performed before MOFs incorporated as shaped bodies can be the preferred adsorbate suitable for use at all levels of applications.

4.2 Recommendations for Future Work

4.2.1 Other Test Methods for Quantifying Mechanical Strength of MOF Pellets

This study provided the first step in characterizing the methods needed to improve the crush strength of MOF pellets. While the axial bulk crush strength was a good method of simulating forces imposed on a pellet in a reactor it is still not adequate, as a single method is not sufficient for accounting for all the requirements needed for the design of industrial bodies. For MOFs to be readily applicable in all areas of interest a set of stringent tests must carried out to satisfy certain requirements. Experiments must also be carried out to account for the fractional break up that occurs during handling, loading and transportation in a converter.

A number of other different methods can be used to quantify the strength of these pellets such as the drop test[44] and the attrition loss test[15]. Although results from these tests were somewhat correlated, they account for different requirements of the pellets for industrial applications. The axial bulk crush strength simulates forces imposed on the pellets in a fixed bed reactor, whereas the drop test simulates the risk of pellet breakup during loading and pneumatic transport. The drop test involves dropping pellets from height of a particular distance and then recording the amount of broken pellets and weights of the resulting fragments. The attrition loss test involves placing pellets in a rotating horizontal cylinder such as a centrifugal ball mill, which is most commonly used device for this test[39]. The attrition loss is then determined by the sieving smaller pieces from the sample and measuring the weight loss by attrition as shown in Equation (7).

$$\%\ \text{Attrition weight loss} = \frac{\text{Fines Weight (g)}}{\text{Sample Weight (g)}} \times 100$$

4.2.2 Investigating Supports with Higher Gas Adsorption Power

Studies should be conducted on developing high strength materials capable of enhancing gas adsorption further than that of the parent MOF material. The addition of a certain range of substrates such as porous oxides and graphite in MOFs can lead to the development of materials with surface properties suitable for an enhanced adsorption of acidic gases even at higher pressures[45]. A reason why such increase in properties is possible is because despite the fact that MOFs have good adsorption properties, their large void spaces are not always effectively utilized. The poor interactions between their pore walls and small gas molecules do not allow their open framework to retain small

adsorbate molecules under standard conditions[46]. To enable stronger interactions between the pore walls and gas molecules, composites with pores sizes similar to those of the target adsorbate molecules can be produced. Petit and Bandosz[47] incorporated graphite oxide (GO) in MOF-5 and observed that at up to 10wt% portion of GO, the textural properties of the material were greatly improved as there were more active sites for reactive adsorption. More recently Zhao et al.[23, 48]incorporated the aminated GO and illustrated how introducing the amine groups to the edges of the GO layers provides extra reactive sites needed for enhanced gas adsorption applications. Other oxides with potential for providing extra active sites particularly those metal oxides which are compatible with the transition metal used in forming UiO-66 and capable of enhancing the dispersive interactions in MOF composites should be investigated upon. Once such oxides have been selected, studies should then be made on incorporating them with UiO-66-PVA to form compacts with exceptional mechanical and adsorption strength.

4.2.3 Other General Recommendations

A variety of polymers with higher decomposition temperatures should be tested. SEM tests should be carried out on all samples to properly investigate the change in particle size and morphology of the UiO-66 crystallites. This will help determine how well the polymer stabilizes the bulk crystalline MOF to mechanical attrition.

APPENDIX A

BULK CRUSH STRENGTH DATA

Sample Calculations for estimating Pelletization Pressure

For applied force of 1400lbs

Diameter of Pellet = 0.5118 inch

Cross-sectional Area $= \frac{\pi d^2}{4}$ =0.2058in^2

Pelletization pressure = $\frac{\text{Applied force}}{\text{Cross-sectional area}}$ = 6802 psi

Similar calculations are carried out for forces applied at 2200 lbs and 3600 lbs to obtain pelletization pressures of 10689 and 17491psi respectively.

UiO-66 Measurements

Table 11. Crush Strength Data for UiO-66 Pellets

Trial / Pelletization Pressure	Crush Strength (lbs)		
	6802 PSI	10689 PSI	17491 PSI
1	10.59	14.43	20.56
2	13.90	20.03	22.37
3	14.81	20.53	24.81
Average	13.10	18.33	22.58

Measurements Collected Using Kaolinite as a Binder

Table 12. Crush Strength Data for UiO-66_Kaolinite 20wt%_800^{o}C Pellets

Trial / Pelletization Pressure	Crush Strength (lbs)		
	6802 PSI	10689 PSI	17491 PSI
Trial 1	4.34	6.26	9.53
Trial 2	4.88	6.17	7.91
Trial 3	-	4.93	7.52
Average	4.61	5.79	8.32

Measurements Collected Using Polyvinyl Alcohol as a Binder

Table 13. Crush Strength Data for PVA Pellets

Trial / Pelletization Pressure	Crush Strength (lbs)	
	10689 PSI	17491 PSI
1	1.50	3.18
2	1.39	2.01
Average	1.45	2.59

Table 14. Crush Strength Data for Uncalcined UiO-66_PVA 7.5wt% Pellets

Trial / Pelletization Pressure	Crush Strength (lbs)		
	6802 PSI	10689 PSI	17491 PSI
1	20.59	26.79	30.57
2	17.47	28.34	30.52
Average	19.03	27.57	30.54

Table 15. Crush Strength Data for Uncalcined UiO-66_PVA 10wt% Pellets

Trial / Pelletization Pressure	Crush Strength (lbs)		
	6802 PSI	10689 PSI	17491 PSI
1	34.68	81.193	84.47
2	45.52	66.33	87.18
Average	40.10	73.76	85.82

Table 16. Crush Strength Data for UiO-66_PVA 10wt% Pellets Calcined at 140^{o}C

Trial/Pelletization Pressure	Crush Strength (lbs)		
	6802 PSI	10689 PSI	17491 PSI
1	45.52	63.82	53.79
2	45.88	62.96	76.50
Average	45.70	63.39	65.14

Table 17. Crush Strength Data for UiO-66_PVA 10wt% Pellets Calcined at 190^{o}C

Trial / Pelletization Pressure	Crush Strength (lbs)		
	6802 PSI	10689 PSI	17491 PSI
1	12.60	29.99	16.58
2	-	19.36	12.85
Average	12.60	24.67	14.71

Table 18. Crush Strength Data for Uncalcined UiO-66_PVA 13wt% Pellets

Trial / Pelletization Pressure	Crush Strength (lbs)		
	6802 PSI	10689 PSI	17491 PSI
1	30.72	30.72	68.06
2	28.39	28.013	63.46
3	16.03	31.151	56.17
Average	25.05	29.96	62.56

Table 19. Crush Strength Data for UiO-66_PVA 13wt% Pellets Calcined at 140^{o}C

Trial / Pelletization Pressure	Crush Strength (lbs)		
	6802 PSI	10689 PSI	17491 PSI
1	24.07	49.20	54.49
2	27.28	27.71	59.16
3	18.42	53.98	67.08
Average	23.26	43.63	60.24

Table 20. Crush Strength Data for UiO-66_PVA 13wt% Pellets Calcined at 190^{o}C

Trial / Pelletization Pressure	Crush Strength (lbs)		
	6802 PSI	10689 PSI	17491 PSI
1	28.68	22.44	35.79
2	25.91	34.58	25.12
3	20.13	15.12	17.24
Average	24.91	24.05	26.05

Measurements Collected Using Tartaric Acid as a Binder

Table 21. Crush Strength Data for Uncalcined UiO-66_Tartaric Acid 10wt% Pellets

Trial / Pelletization Pressure	Crush Strength (lbs)		
	6802 PSI	10689 PSI	17491 PSI
1	9.71	8.63	19.03
2	5.71	10.82	7.60
Average	7.71	9.73	13.31

Table 22. Crush Strength Data for UiO-66_Tartaric Acid 10wt% Pellets Calcined at 140 ^{o}C

Trial / Pelletization Pressure	Crush Strength (lbs)		
	6802 PSI	10689 PSI	17491 PSI
1	7.22	12.40	12.95
2	11.42	5.86	16.82
Average	9.32	9.13	14.89

Table 23. Crush Strength Data for UiO-66_Tartaric Acid 13wt% Pellets Calcined at 140 ^{o}C

Trial / Pelletization Pressure	Crush Strength (lbs)		
	6802 PSI	10689 PSI	17491 PSI
1	9.72	9.08	19.27
2	5.57	7.42	12.51
3	13.73	19.08	12.74
Average	9.67	11.86	14.84

APPENDIX B

RAW SINGLE COMPONENT GAS ADSORPTION-DESORPTION DATA

All raw isotherm data were collected at 298 K while sample activations were carried out insitu under vacuum at 493 K for 12 to 15 hours.

UiO-66 Data

UiO-66-S1

Molar mass of CO_2 (g/mmol) = 0.04401

Table 24. Adsorption-Desorption Data for UiO-66-S1

Adsorption			Desorption		
Weight (mg)	P (bar)	mmol CO_2/g MOF	Weight (mg)	P (bar)	mmol CO_2/g MOF
26.6806	0.015823	0	34.69973	14.99872	6.797547
26.78281	0.052172	0.087046	32.92733	7.498119	5.288111
26.8505	0.079567	0.144693	30.20939	2.50079	2.973421
26.91505	0.104557	0.199666	27.76521	0.499052	0.891874
27.61362	0.454684	0.794592	26.95434	0.099613	0.201309
28.47711	0.999386	1.529969	26.71796	0.004865	0
30.13125	2.49932	2.938691			
31.82298	4.998586	4.379426			
32.90382	7.530325	5.299906			
33.66441	9.997652	5.947651			
34.24247	12.49879	6.439946			
34.69973	14.99872	6.829365			

UiO-66-S2

Molar mass of CO_2 (g/mmol) = 0.04401

Table 25. Adsorption-Desorption Data for UiO-66-S2

Adsorption			Desorption		
Weight (mg)	P (bar)	mmol CO_2/g MOF	Weight (mg)	P (bar)	mmol CO_2/g MOF
26.01466	0.012749	0	33.68456	14.99846	6.672525
26.1196	0.055513	0.091658245	31.91656	7.496516	5.12969
26.17987	0.080102	0.144300159	29.31541	2.498652	2.859812
26.22768	0.100682	0.186059075	27.02158	0.495844	0.858115
26.34109	0.148524	0.285115312	26.27622	0.098276	0.207681
26.53079	0.250622	0.450805889	26.03823	0.003261	0
26.89155	0.451744	0.765906217			
27.7109	1.00246	1.481554997			
29.27018	2.497716	2.843484367			
30.88675	5.039746	4.255452816			
31.89972	7.49852	5.140216036			
32.65026	9.998454	5.795763769			
33.23152	12.49679	6.303456465			
33.68456	14.99846	6.699157354			

For isotherm data collected for MOF composites containing a binder, adsorption and desorption loadings were normalized with respect to the amount of MOF present in the composite for easy comparisons. Normalization was done by multiplying the composition of MOF present to the total weights obtained from the isotherm data. The resulting weights were then used to determine the respective loadings for the different samples.

CO2 Adsorption Data Collected with Kaolinite as a Binder

UiO-66-S1_Kaolinite 20wt%_800 °C

Molar mass of CO_2 (g/mmol) = 0.04401

Table 26. Adsorption-Desorption Data for UiO-66-S1_K800C_20wt%

Adsorption			Desorption		
Weight (mg)	P (bar)	mmol CO_2/g MOF	Weight (mg)	P (bar)	mmol CO_2/g MOF
41.81507	0.015155	0	41.97887	15.00313	0.114343
41.81601	0.054444	0.000638489	41.90983	7.498921	0.067443
41.81849	0.078498	0.002323015	41.85089	2.501458	0.027404
41.81919	0.105359	0.002798485	41.82164	0.488762	0.007534
41.82033	0.155606	0.003572823	41.81373	0.097207	0.00216
41.82224	0.249419	0.00487018	41.81055	0.002459	0
41.82635	0.451611	0.007661872			
41.83519	0.999921	0.013666389			
41.85476	2.497716	0.026959195			
41.88071	5.023709	0.044585577			
41.90457	7.501326	0.060792339			
41.92804	10.00674	0.076734196			
41.95409	12.49973	0.094428502			
41.97887	15.00313	0.111260169			

CO2 Adsorption Data Collected with PVA as a Binder

UiO-66-S2_PVA 7.5wt%

Molar mass of CO_2 (g/mmol) = 0.04401

Table 27. Adsorption-Desorption Data for UiO-66-S2_PVA 7.5wt%

Adsorption			Desorption		
Weight (mg)	P (bar)	mmol CO_2/g MOF	Weight (mg)	P (bar)	mmol CO_2/g MOF
27.16328	0.001657	0	34.11954	15.00046	6.232231275
27.20996	0.015288	0.042214	32.50293	7.493175	4.773061264
27.30058	0.057785	0.124164	30.14667	2.498652	2.646275007
27.33891	0.075692	0.158827	28.09429	0.49825	0.793774189
27.38842	0.100682	0.2036	27.41965	0.098009	0.184836686
27.98256	0.453482	0.740896	27.21487	0.005533	0
28.71442	0.999252	1.402735			
30.12075	2.498117	2.674515			
31.56361	4.995512	3.97933			
32.49532	7.491571	4.821899			
33.17365	10.00166	5.43533			
33.70597	12.50186	5.91672			
34.11954	15.00046	6.290722			

UiO-66-S2_PVA 10wt%

Molar mass of CO_2 (g/mmol) = 0.04401

Table 28. Adsorption-Desorption Data for UiO-66-S2_PVA 10wt%

Adsorption			Desorption		
Weight (mg)	P (bar)	mmol CO_2/g MOF	Weight (mg)	P (bar)	mmol CO_2/g MOF
25.15589	0.001257	0	31.40492	14.98924	6.222734
25.20277	0.016758	0.047049394	29.95876	7.493442	4.773599
25.2887	0.058586	0.133289891	27.84173	2.496513	2.652215
25.32192	0.075291	0.166629927	26.01886	0.497849	0.825595
25.38026	0.106562	0.22518073	25.39736	0.09694	0.202816
25.91499	0.451611	0.761842903	25.19496	0.003796	0
26.56789	0.997248	1.417102068			
27.81566	2.503062	2.669380713			
29.09403	4.994978	3.952369927			
29.95712	7.489566	4.818578584			
30.5682	9.993108	5.431866637			
31.03704	12.50173	5.902400726			
31.40492	14.98924	6.27161001			

UiO-66-S1_PVA 13wt%

Molar mass of CO_2 (g/mmol) = 0.04401

Table 29. Adsorption-Desorption Data for UiO-66-S1_PVA 13wt%

Adsorption			Desorption		
Weight (mg)	P (bar)	mmol CO_2/g MOF	Weight (mg)	P (bar)	mmol CO_2/g MOF
26.78304	0.002727	0	33.48521	15.005	6.467716383
26.83079	0.015957	0.046563207	32.00129	7.493576	5.023686145
26.91074	0.051103	0.124526106	29.76897	2.499453	2.851373903
26.97861	0.078632	0.190709244	27.74563	0.499453	0.882423999
27.03157	0.103889	0.24235296	27.05075	0.098677	0.206223306
27.63889	0.454284	0.834578445	26.83883	0.0058	0
28.37713	1.002326	1.554470005			
29.74887	2.499587	2.892116364			
31.1222	4.993775	4.231313204			
31.9938	7.491303	5.081250194			
32.62366	9.998188	5.695455463			
33.1115	12.50681	6.17117054			
33.48521	15.005	6.535592239			

UiO-66-S1_PVA 13wt%_6802psi

Molar mass of CO_2 (g/mmol) = 0.04401

Table 30. Adsorption-Desorption Data for UiO-66-S1_PVA 13wt%_6802psi

Adsorption			Desorption		
Weight (mg)	P (bar)	mmol CO_2/g MOF	Weight (mg)	P (bar)	mmol CO_2/g MOF
29.43388	0.001524	0	36.09763	15.0022	5.862281
29.46489	0.014353	0.027515894	34.65854	7.492907	4.587361
29.53018	0.056983	0.085449229	32.46052	2.499854	2.640089
29.57352	0.080236	0.123905819	30.42026	0.497181	0.83258
29.61924	0.105359	0.164474239	29.70211	0.099212	0.196356
30.20333	0.45856	0.682750879	29.48047	0.005399	0
30.97	0.999653	1.363034999			
32.38837	2.502393	2.621587685			
33.77243	4.995512	3.84969631			
34.63829	7.49558	4.617994024			
35.26106	9.996449	5.170592327			
35.73454	12.50213	5.590722142			
36.09763	15.0022	5.912900343			

UiO-66-S1_PVA 13wt%_10689psi

Molar mass of CO_2 (g/mmol) = 0.04401

Table 31. Adsorption-Desorption Data for UiO-66-S1_PVA 13wt%_10689psi

Adsorption			Desorption		
Weight (mg)	P (bar)	mmol CO_2/g MOF	Weight (mg)	P (bar)	mmol CO_2/g MOF
32.59546	0.001524	0	39.81765	15.00126	5.741445524
32.64448	0.015021	0.039277657	38.28717	7.495848	4.516881187
32.74911	0.056181	0.123113259	35.90888	2.500389	2.613968951
32.799	0.074756	0.16308801	33.67124	0.499854	0.823593288
32.85655	0.100548	0.209200396	32.88451	0.09988	0.194116587
33.56266	0.458293	0.774976534	32.6419	0.0058	0
34.38557	1.0054	1.434339581			
35.88521	2.500389	2.635937812			
37.35797	4.99725	3.815998234			
38.28221	7.489834	4.556552733			
38.9339	9.998722	5.078724422			
39.43144	12.50253	5.477382222			
39.81765	15.00126	5.786835993			

UiO-66-S1_PVA 13wt%_17491psi

Molar mass of CO_2 (g/mmol) = 0.04401

Table 32. Adsorption-Desorption Data for UiO-66-S1_PVA 13wt%_17491psi

Adsorption			Desorption		
Weight (mg)	P (bar)	mmol CO_2/g MOF	Weight (mg)	P (bar)	mmol CO_2/g MOF
27.70154	0.001791	0	33.63391	15.001	5.548339
27.74669	0.015823	0.042567997	32.35656	7.493175	4.345738
27.83817	0.058987	0.128816512	30.41107	2.498785	2.514095
27.86843	0.074222	0.157346027	28.58844	0.497983	0.798122
27.93358	0.107497	0.21877028	27.9404	0.098009	0.188004
28.49542	0.456021	0.748480218	27.74071	0.006335	0
29.17224	1.004999	1.386594771			
30.39326	2.499052	2.537788044			
31.59463	4.995512	3.670455045			
32.35361	7.492239	4.386031097			
32.89315	10.00006	4.89471631			
33.31268	12.49438	5.29025456			
33.63391	15.001	5.593114312			

CH_4 Adsorption Data Collected with PVA as a Binder

UiO-66-S1_PVA 13wt%_17491psi

Molar mass of CH_4 (g/mmol) = 0.01604

Table 33. CH_4 Adsorption-Desorption Data for UiO-66-S1_PVA 13wt%_17491psi

Adsorption			Desorption		
Weight (mg)	P (bar)	mmol CO_2/g MOF	Weight (mg)	P (bar)	mmol CO_2/g MOF
29.88893	0.00139	0	31.39091	14.99231	3.532832
29.93254	0.016357	0.104556756	30.90567	7.493442	2.370503
29.98275	0.055112	0.224937283	30.39355	2.499721	1.143788
30.00036	0.079835	0.267157977	30.03956	0.499987	0.295852
30.0145	0.106963	0.301059205	29.93515	0.097876	0.045752
30.1174	0.453615	0.547766158	29.91605	0.007938	0
30.29829	1.000188	0.981457322			
30.52762	2.499988	1.531285365			
30.84691	4.992839	2.296796183			
31.03901	7.491705	2.757363781			
31.18671	9.997251	3.111480564			
31.29689	12.49812	3.375641615			
31.39091	14.99231	3.601058406			

CO_2 Adsorption Data Collected with Tartaric Acid as a Binder

UiO-66-S1_Tartaric Acid 7.5wt%

Molar mass of CO_2 (g/mmol) = 0.04401

Table 34. Adsorption-Desorption Data for UiO-66-S1_TA_7.5wt%

Adsorption			Desorption		
Weight (mg)	P (bar)	mmol CO_2/g MOF	Weight (mg)	P (bar)	mmol CO_2/g MOF
23.40231	0.000054	0	28.8211	15.00273	5.641582
23.43927	0.012081	0.038795391	27.72362	7.497317	4.491366
23.54222	0.056582	0.146857769	25.95149	2.49932	2.634081
23.59012	0.078899	0.197136428	24.28143	0.499987	0.88377
23.63864	0.103355	0.248065875	23.65105	0.095737	0.223099
24.17838	0.449874	0.814608742	23.43818	0.005667	0
24.80573	1.00099	1.47311222			
25.92751	2.504131	2.650598522			
27.02772	5.00166	3.805443682			
27.71758	7.490769	4.529561335			
28.19695	9.994847	5.032736296			
28.55334	12.49866	5.406824213			
28.8211	15.00273	5.687880866			

UiO-66-S1_Tartaric Acid 10wt%

Molar mass of CO_2 (g/mmol) = 0.04401

Table 35. Adsorption-Desorption Data for UiO-66-S2_Tartaric Acid 10wt%

Adsorption			Desorption		
Weight (mg)	P (bar)	mmol CO_2/g MOF	Weight (mg)	P (bar)	mmol CO_2/g MOF
26.25605	0.000722	0	31.47058	14.99324	4.976171
26.30742	0.015422	0.049395	30.38952	7.49598	3.937968
26.41223	0.056983	0.150177	28.68127	2.500522	2.29744
26.4454	0.074222	0.182072	27.1149	0.498517	0.793168
26.50917	0.105894	0.24339	26.5096	0.099212	0.211864
27.04263	0.454551	0.756344	26.28899	0.005533	0
27.6332	1.005266	1.324213			
28.67941	2.503062	2.330208			
29.72935	4.997517	3.339789			
30.39244	7.493843	3.97739			
30.85682	9.997519	4.42392			
31.20979	12.50079	4.763322			
31.47058	14.99324	5.014087			

REFERENCES

1. Furukawa, H., et al., *Ultrahigh Porosity in Metal-Organic Frameworks.* Science 2010. **329**(5990): p. 424-428.

2. Wu, H., et al., *Unusual and Highly Tunable Missing-Linker Defects in Zirconium Metal-Organic Framework UiO-66 and Their Important Effects on Gas Adsorption.* Journal of the American Chemical Society, 2013. **135**(28): p. 10525-10532.

3. Duerinck, T., et al., *Understanding Hydrocarbon Adsorption in the UiO-66 Metal-Organic Framework: Separation of (Un)saturated Linear, Branched, Cyclic Adsorbates, Including Stereoisomers.* Journal of Physical Chemistry C, 2013. **117**(24): p. 12567-12578.

4. Li, J.R., R.J. Kuppler, and H.C. Zhou, *Selective gas adsorption and separation in metal-organic frameworks.* Chemical Society Reviews, 2009. **38**(5): p. 1477-1504.

5. Murray, L.J., M. Dinca, and J.R. Long, *Hydrogen storage in metal-organic frameworks.* Chemical Society Reviews, 2009. **38**(5): p. 1294-1314.

6. Tagliabue, M., et al., *Methane storage on CPO-27-Ni pellets.* Journal of Porous Materials, 2011. **18**(3): p. 289-296.

7. Lee, J., et al., *Metal-organic framework materials as catalysts.* Chemical Society Reviews, 2009. **38**(5): p. 1450-1459.

8. Taylor-Pashow, K.M.L., et al., *Postsynthetic Modifications of Iron-Carboxylate Nanoscale Metal-Organic Frameworks for Imaging and Drug Delivery.* Journal of the American Chemical Society, 2009. **131**(40): p. 14261-+.

9. Deutschmann, O., et al., *Heterogeneous Catalysis and Solid Catalysts*. 2009, Weinheim: Wiley-VCH.

10. Finsy, V., et al., *Separation of CO2/CH4 mixtures with the MIL-53(Al) metal-organic framework.* Microporous and Mesoporous Materials, 2009. **120**(3): p. 221-227.

11. Wu, H., T. Yildirim, and W. Zhou, *Exceptional Mechanical Stability of Highly Porous Zirconium Metal-Organic Framework UiO-66 and Its Important Implications.* Journal of Physical Chemistry Letters, 2013. **4**(6): p. 925-930.

12. Finney, K.N., V.N. Sharifi, and J. Swithenbank, *Fuel Pelletization with a Binder: Part I - Identification of a Suitable Binder for Spent Mushroom Compost-Coal Tailing Pellets.* Energy & Fuels, 2009. **23**: p. 3195-3202.

13. *Kirk-Othmer Encyclopedia of Chemical Technology*. 1983, John Wiley & Sons: New York.

14. Sulaymon, A.H. and A.S. Mahdi, *Spherical zeolite-binder agglomerates.* Chemical Engineering Research & Design, 1999. **77**(A4): p. 342-350.

15. Satterfield, C.N., *Heterogeneous Catalysis in Practice*. 1980, United States: McGraw-Hill.

16. Kim, J., et al., *Bench-scale preparation of Cu-3(BTC)(2) by ethanol reflux: Synthesis optimization and adsorption/catalytic applications.* Microporous and Mesoporous Materials, 2012. **161**: p. 48-55.

17. Liu, J., P.K. Thallapally, and D. Strachan, *Metal-Organic Frameworks for Removal of Xe and Kr from Nuclear Fuel Reprocessing Plants.* Langmuir, 2012. **28**(31): p. 11584-11589.

18. Liu, D., et al., *MOF-5 composites exhibiting improved thermal conductivity.* International Journal of Hydrogen Energy, 2012. **37**(7): p. 6109-6117.

19. Peterson, G.W., et al., *Effects of pelletization pressure on the physical and chemical properties of the metal-organic frameworks Cu-3(BTC)(2) and UiO-66.* Microporous and Mesoporous Materials, 2013. **179**: p. 48-53.

20. Tan, J.C. and A.K. Cheetham, *Mechanical properties of hybrid inorganic-organic framework materials: establishing fundamental structure-property relationships.* Chemical Society Reviews, 2011. **40**(2): p. 1059-1080.

21. Graham, A.J., et al., *The effect of pressure on Cu-btc: framework compression vs. guest inclusion.* Chemical Communications, 2012. **48**(10): p. 1535-1537.

22. Liu, Y.Y., Z.Y.U. Wang, and H.C. Zhou, *Recent advances in carbon dioxide capture with metal-organic frameworks.* Greenhouse Gases-Science and Technology, 2012. **2**(4): p. 239-259.

23. Zhao, Y.X., H.L. Ding, and Q. Zhong, *Synthesis and characterization of MOF-aminated graphite oxide composites for CO2 capture.* Applied Surface Science, 2013. **284**: p. 138-144.

24. Millward, A.R. and O.M. Yaghi, *Metal-organic frameworks with exceptionally high capacity for storage of carbon dioxide at room temperature.* Journal of the American Chemical Society, 2005. **127**(51): p. 17998-17999.

25. Bae, Y.S. and R.Q. Snurr, *Development and Evaluation of Porous Materials for Carbon Dioxide Separation and Capture.* Angewandte Chemie-International Edition, 2011. **50**(49): p. 11586-11596.

26. Cunha, D., et al., *Rationalization of the entrapping of bioactive molecules into a series of functionalized porous zirconium terephthalate MOFs.* Journal of Materials Chemistry B, 2013. **1**(8): p. 1101-1108.

27. Biswas, S. and P. Van der Voort, *A General Strategy for the Synthesis of Functionalised UiO-66 Frameworks: Characterisation, Stability and CO2 Adsorption Properties.* European Journal of Inorganic Chemistry, 2013(12): p. 2154-2160.

28. Ilic, B.R., A.A. Mitrovic, and L.R. Milicic, *Thermal Treatment of Kaolin Clay to obtain Metakaolin.* Hemijska Industrija, 2010. **64**(4): p. 351-356.

29. Kakali, G., et al., *Thermal treatment of kaolin: the effect of mineralogy on the pozzolanic activity.* Applied Clay Science, 2001. **20**(1-2): p. 73-80.

30. *PVA for Paper Industry-Perry Chemical Corporation*. [cited October 27 2013; Available from: http://www.perrychem.com/files/PVA_English_2009_.pdf

31. *Mowiol Clariant*. [cited October 27, 2013; Available from: http://www2.cbm.uam.es/confocal/Manuales/mowiol.pdf.

32. Vyas, R.K., Shashi, and S. Kumar, *Determination of micropore volume and surface area of zeolite molecular sieves by D-R and D-A equations: A comparative study.* Indian Journal of Chemical Technology, 2004. **11**(5): p. 704-709.

33. Walton, K.S. and R.Q. Snurr, *Applicability of the BET method for determining surface areas of microporous metal-organic frameworks.* Journal of the American Chemical Society, 2007. **129**(27): p. 8552-8556.

34. *Standard Test Method for Single Pellet Crush Strength of Formed Catalysts and Catalyst Carriers*, in *ASTM standard D4179*. 2011, ASTM International: West Conshohocken, PA.

35. Valenzano, L., et al., *Disclosing the Complex Structure of UiO-66 Metal Organic Framework: A Synergic Combination of Experiment and Theory.* Chemistry of Materials, 2011. **23**(7): p. 1700-1718.

36. Lau, C.H., R. Babarao, and M.R. Hill, *A route to drastic increase of CO_2 uptake in Zr metal organic framework UiO-66.* Chemical Communications, 2013. **49**(35): p. 3634-3636.

37. Biswas, S., et al., *Enhanced selectivity of CO2 over CH4 in sulphonate-, carboxylate- and iodo-functionalized UiO-66 frameworks.* Dalton Transactions, 2013. **42**(13): p. 4730-4737.

38. Jasuja, H. and K.S. Walton, *Experimental Study of CO2, CH4, and Water Vapor Adsorption on a Dimethyl-Functionalized Ui0-66 Framework.* Journal of Physical Chemistry C, 2013. **117**(14): p. 7062-7068.

39. Ugal, J.R., M. Mustafa, and A.A. Abdulhadi, *Preparation of Zeolite Type 13X from Locally Available Raw Materials.* Iraqi Journal of Chemical and Petroleum Engineering, 2008. **9**(1): p. 51-56.

40. Mohammed, A.-H.A. and Z.K. Nassrullah, *Preparation and Formation of Zeolite 5A from Local Kaolin Clay for Drying and Desuphurization of Liquefied Petroleum Gas.* Iraqi Journal of Chemical and Petroleum Engineering, 2013. **14**(1): p. 1-13.

41. Baklouti, S., et al., *Binder burnout and evolution of the mechanical strength of dry-pressed ceramics containing poly(vinyl alcohol).* Journal of the European Ceramic Society, 2001. **21**(8): p. 1087-1092.

42. Yang, Q.Y., et al., *Functionalizing porous zirconium terephthalate UiO-66(Zr) for natural gas upgrading: a computational exploration.* Chemical Communications, 2011. **47**(34): p. 9603-9605.

43. Wiersum, A.D., et al., *An Evaluation of UiO-66 for Gas-Based Applications.* Chemistry-an Asian Journal, 2011. **6**(12): p. 3270-3280.

44. Gani, R., K. Dam-Johansen, and K.M. Ng, *Chemical Product Design: Towards a Perspective through Case Studies*. First edition ed. 2007, Netherlands: Elsevier.

45. O'Neill, L.D., H.F. Zhang, and D. Bradshaw, *Macro-/microporous MOF composite beads.* Journal of Materials Chemistry, 2010. **20**(27): p. 5720-5726.

46. Petit, C. and T.J. Bandosz, *MOF-Graphite Oxide Composites: Combining the Uniqueness of Graphene Layers and Metal-Organic Frameworks.* Advanced Materials, 2009. **21**(46): p. 4753-+.

47. Petit, C. and T.J. Bandosz, *MOF-Graphite Oxide Composites: Combining the Uniqueness of Graphene Layers and Metal-Organic Frameworks.* Advanced Materials, 2009. **21**(46): p. 4753-4757.

48. Zhao, Y.X., et al., *Aminated graphite oxides and their composites with copper-based metal-organic framework: in search for efficient media for CO2 sequestration.* Rsc Advances, 2013. **3**(25): p. 9932-9941.